

Searches of a Cosmological Gravitational-Wave Background with 3G Detectors: Probing the Very Early Universe

Ashish Sharma^{1,2}

Advisor: Jan Harms^{1,2}

PhD Thesis Defence

1 February 2020



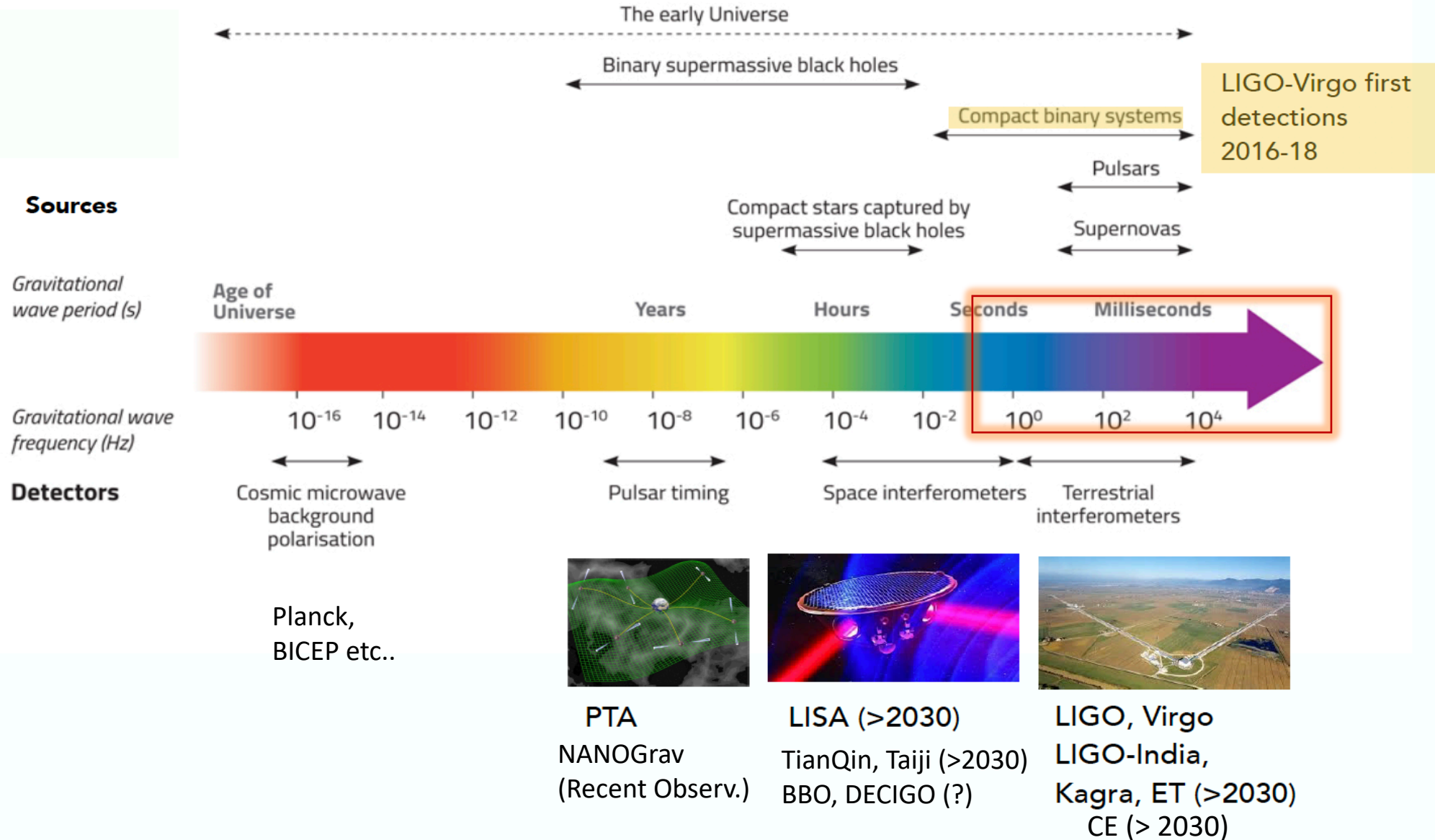
¹Gran Sasso Science Institute (GSSI), I–67100 L'Aquila, Italy
²INFN, Laboratori Nazionali del Gran Sasso, I–67100 Assergi, Italy



Overview

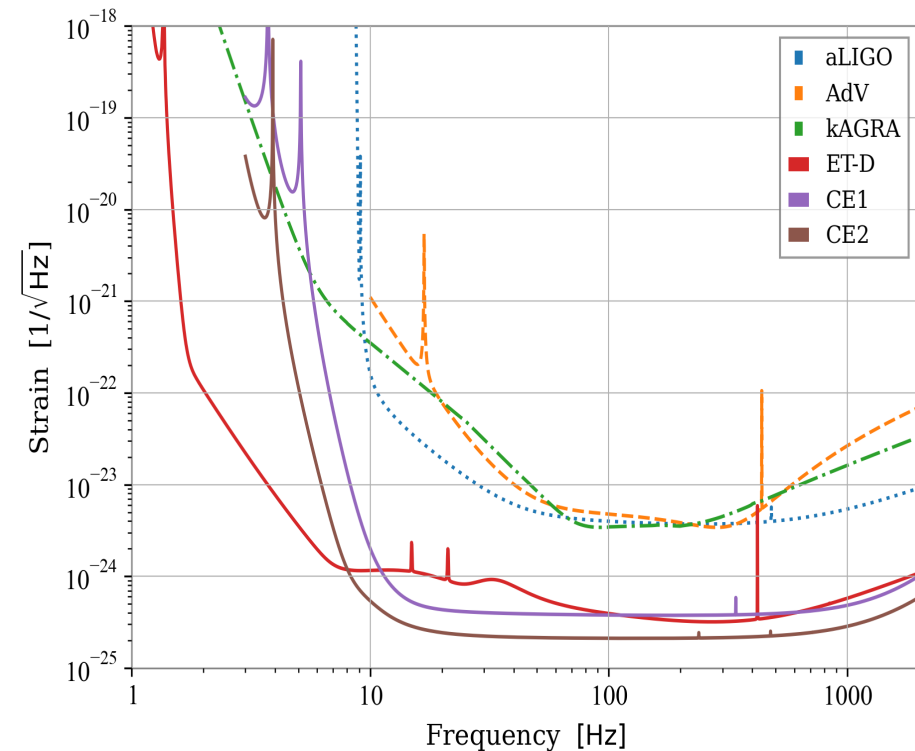
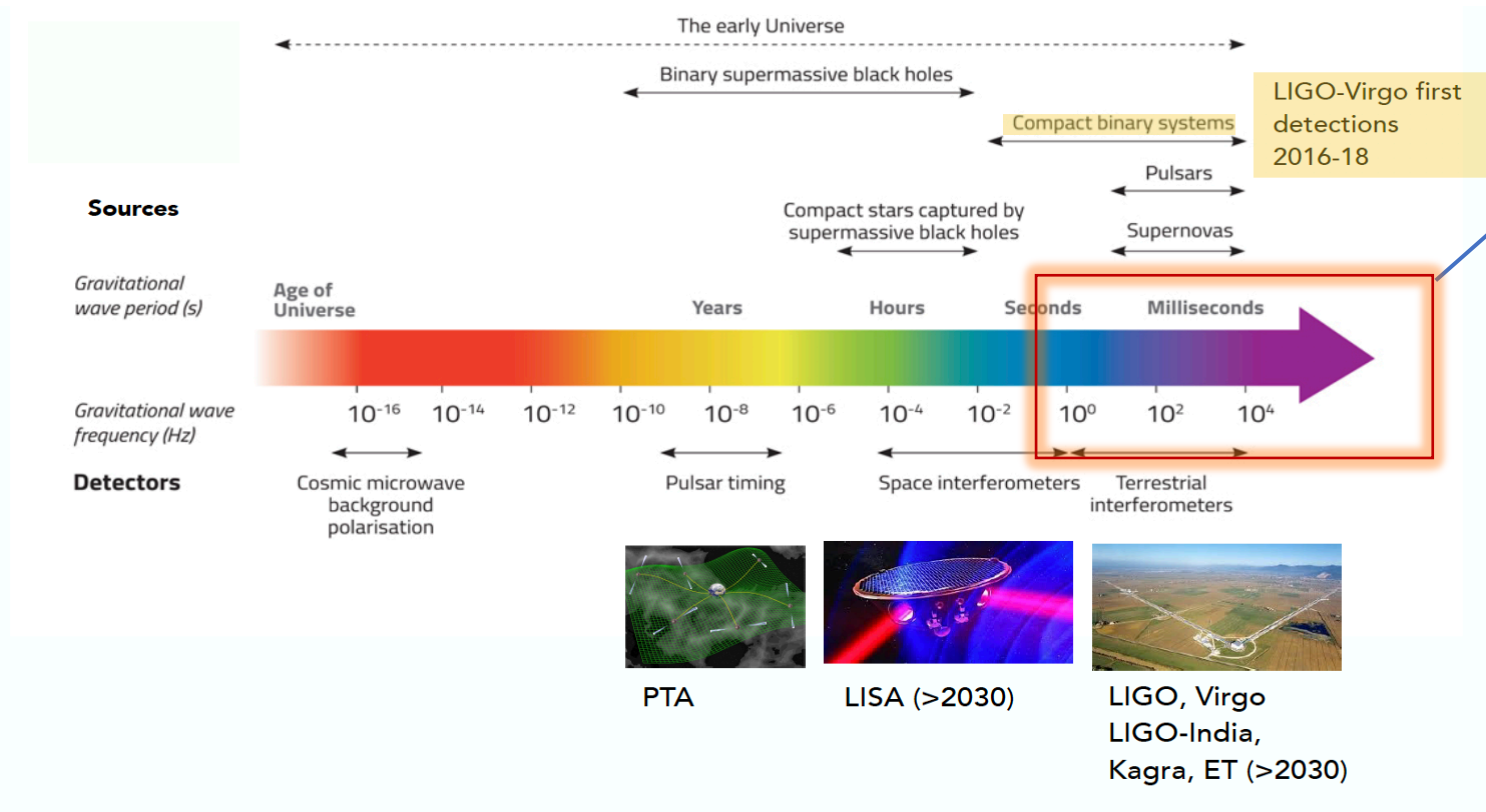
- Introduction
 - Future perspective of GW physics
- Sources and background detection
 - GW sources for 3G detectors
 - Astrophysical background
 - Cosmological background
- Stochastic background and 3G detectors
 - Challenges in background detection
 - Subtraction-noise projection method
 - Results
- O3 data analysis
 - O3 run dataset
 - Data cuts
 - Point estimates
 - Upper limits from O3 analysis
- Conclusion

Stepping into new epoch of GW physics



What we have in future?

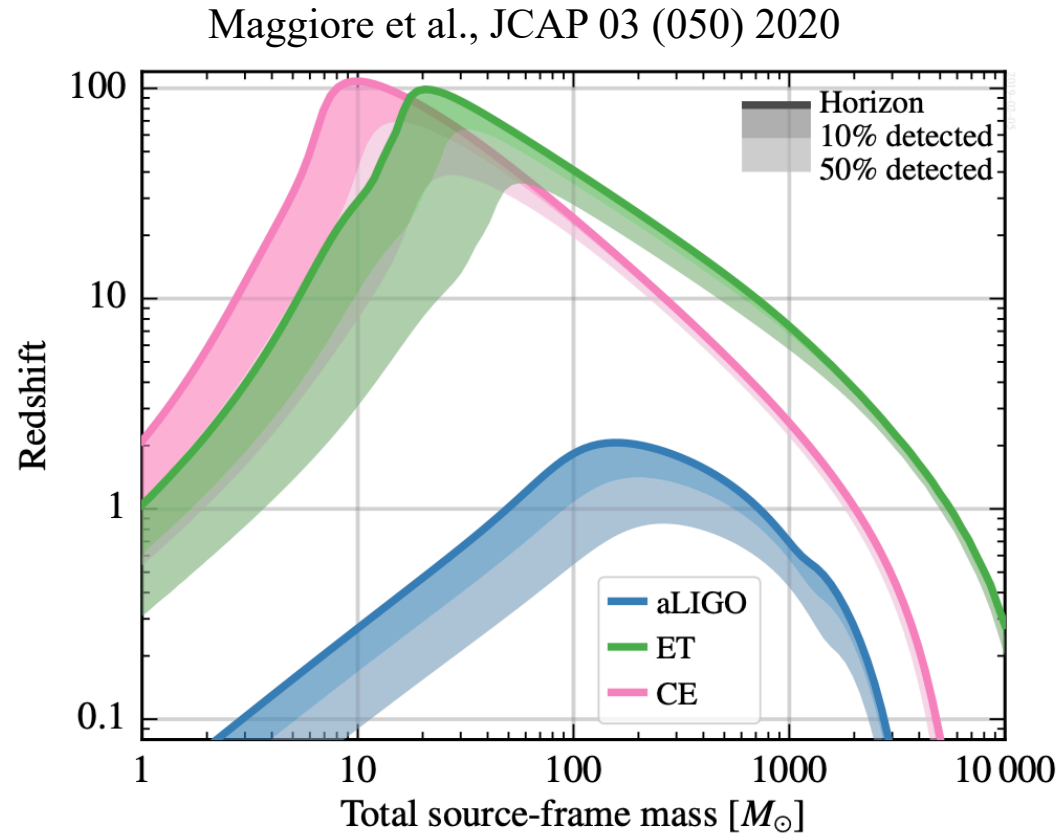
- Einstein Telescope (ET) and Cosmic Explorer (CE)
- Operation expected to be 2035 +
- 10 times better strain sensitivity than current GW detectors.
- Probing the lower frequencies up to 2-10 Hz.



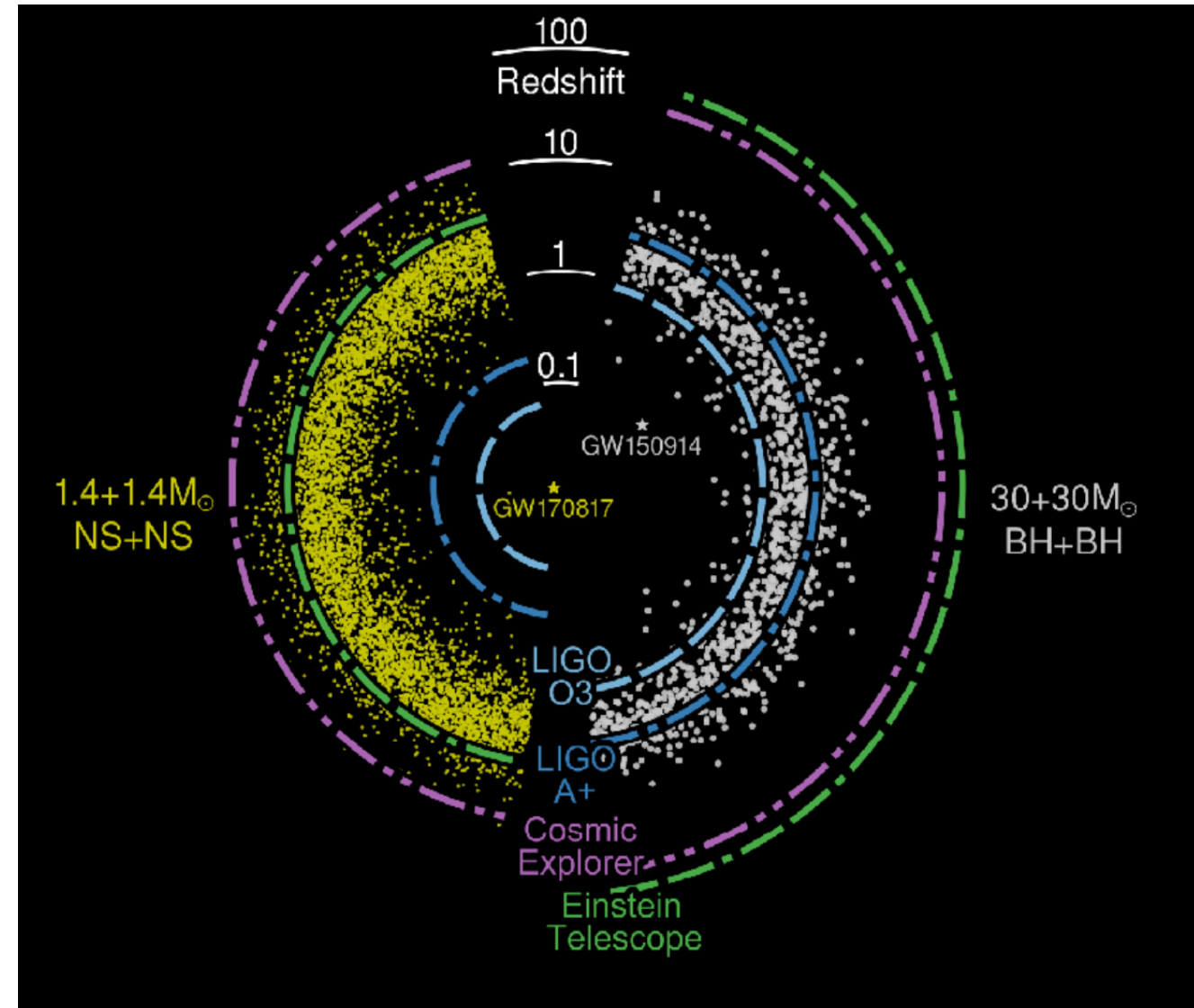
The sensitivity curve for aLIGO and AdV GW detectors with anticipated sensitivity curves for future GW detectors.

Scientific reach of 3G detectors

ET-0015A-20



astrophysical reach of non-spinning equal mass
binaries accessible with aLIGO, ET, and CE GW detectors.



GW sources for 3G detectors

- More and more astrophysical observations
 - BBH ($\sim 10^5$ per year)
 - BNS ($\sim 10^6$ per year)
 - NS-BH
 - IMBH binaries ($M_{\odot} > 100 M_{\odot}$)
 - SNe's
 - Magnetars
 - More exotic signals
- Cosmological observations
 - First order phase transitions
 - Cosmic strings
 - Inflationary background signatures
 - PBHs

What we will detect?

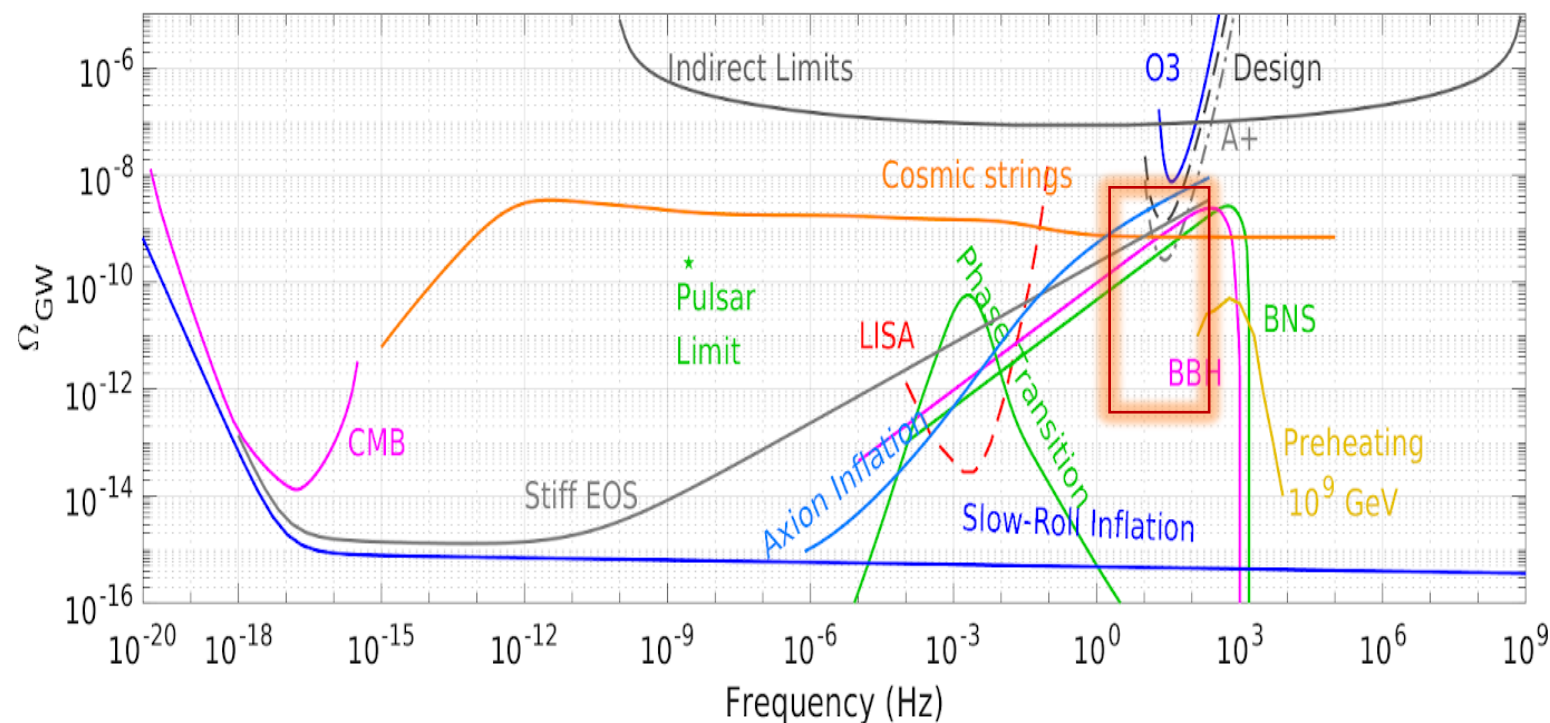
- **Two types of astrophysical measurements**

Astrophysical observable	Measurable quantity/parameters	We will learn about
Resolvable GW sources	GW signal waveform as a function of time and frequency.	Parameters characterizing binary object; mass, spin, eccentricity, luminosity distance and many more...
Unresolved GW sources background	More waveforms, intensity of astrophysical background and polarization, direction and frequency dependence.	Redshift distribution, formation and stellar evolution, distribution of astrophysical sources.

Astrophysical stochastic background

$$\Omega_{GW}(f) = \frac{f}{\rho_c} \frac{d\rho_{GW}(f)}{df} = \int dz \underbrace{\frac{dE(z)}{df}}_{\text{Energy flux spectrum}} \underbrace{R(z)}_{\text{\# density of binary sources}} \underbrace{\frac{N(z)}{H(z)}}_{\text{event rate}} \quad (1)$$

- ρ_c = critical energy density
- ρ_{GW} = GW energy density
- $H(z)$ = Hubble constant



Upper limits on Ω_{GW}

Limits on Ω_{GW} (from O2)

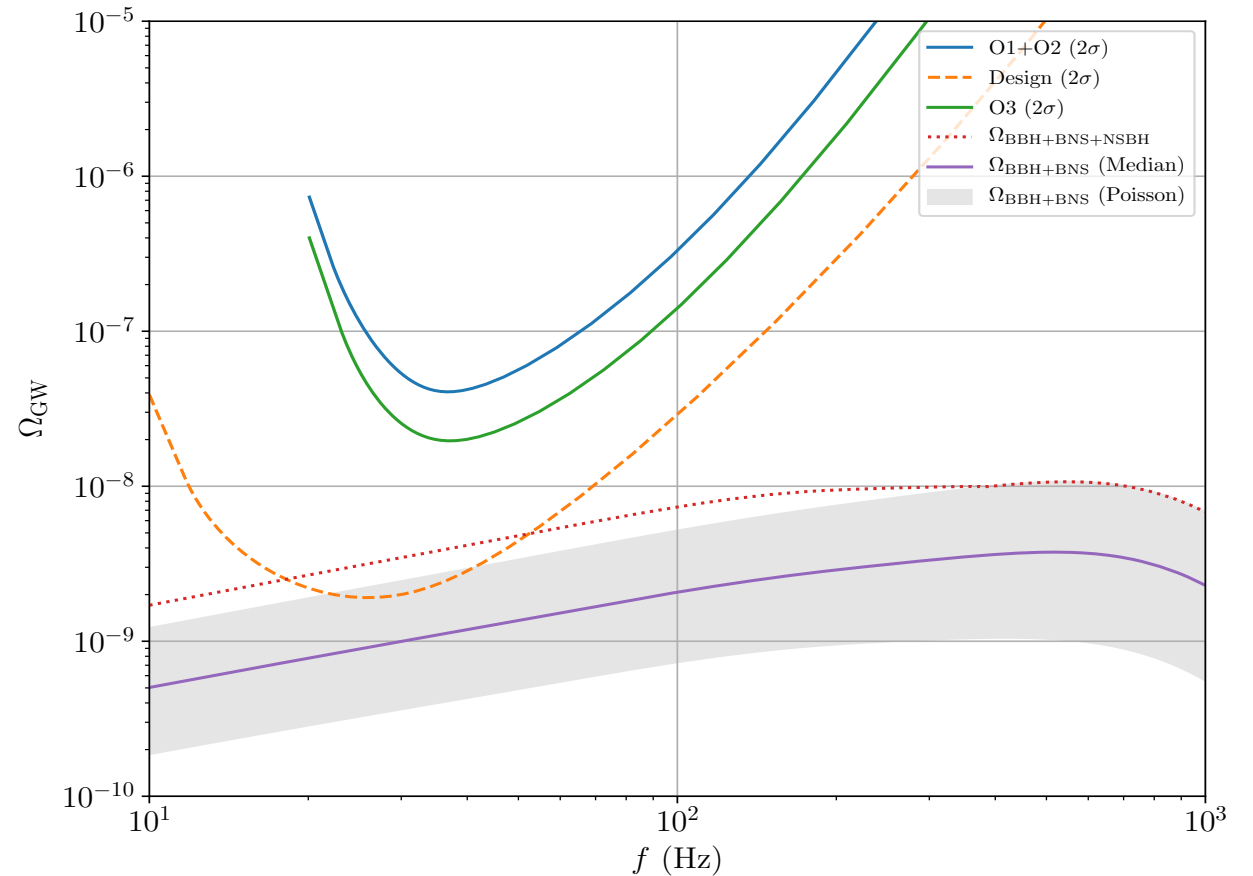
For BBHs

- GW150914: 1.1×10^{-9} ($f = 25$ Hz)

For BNS

- GW170817: 1.8×10^{-9} ($f = 25$ Hz)

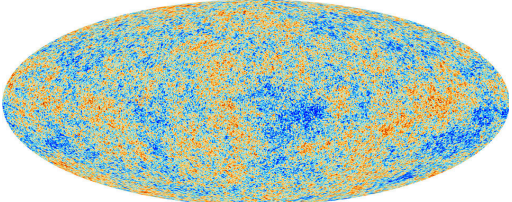
B. Abbott et al., PRD 100 (061101) 2019



Detection of astrophysical stochastic background is plausible when design sensitivity is reached.

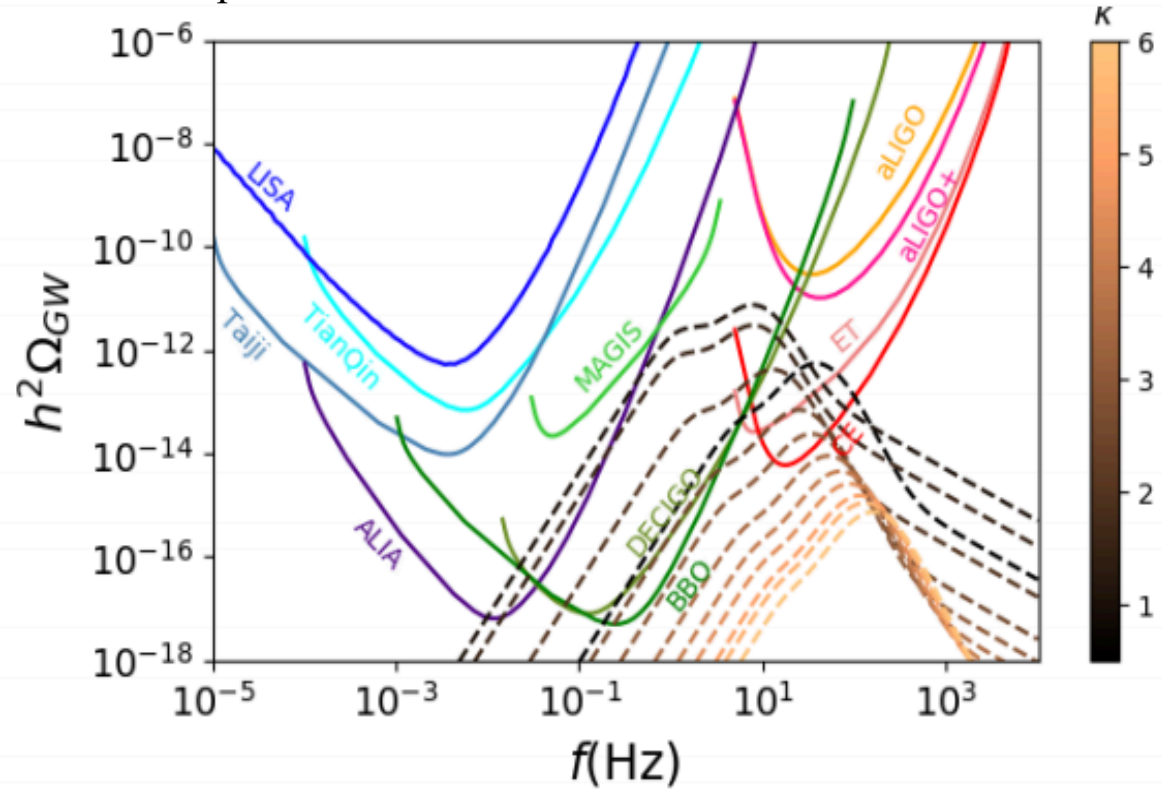
What we will detect?

- **Cosmological background**

Cosmological observable	Measurable quantity/parameters	We will learn about
<p>Primordial signature of universe, i.e. cosmological background</p> 	<p>GW signal from the early universe processes, intensity of background and polarization, direction and frequency dependence.</p>	<p>Parameters associated with cosmological processes.</p> <p>Isotropy or anisotropy of the universe, Gaussian or non- Gaussian behaviour, and many more aspects.</p>

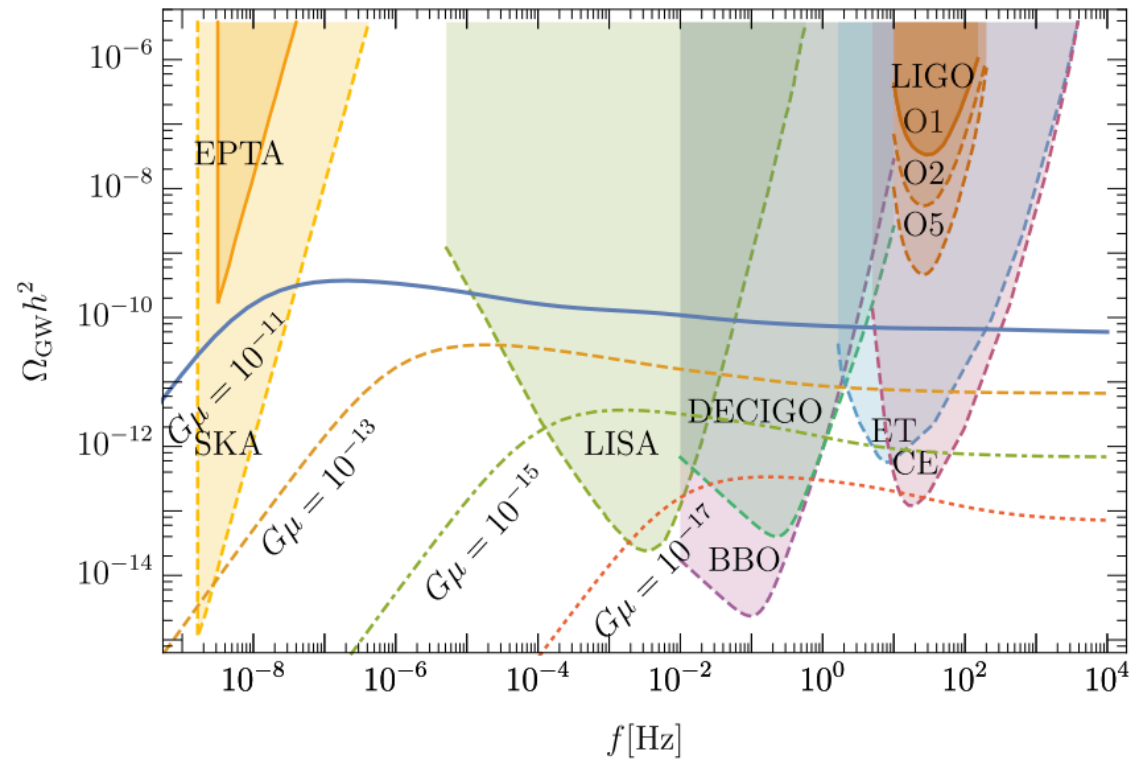
Cosmological backgrounds

First order phase transition parameter κ gives the amount of energy converted to GWs during the phase transitions.



PS Dev et al., JCAP 11(006) 2019

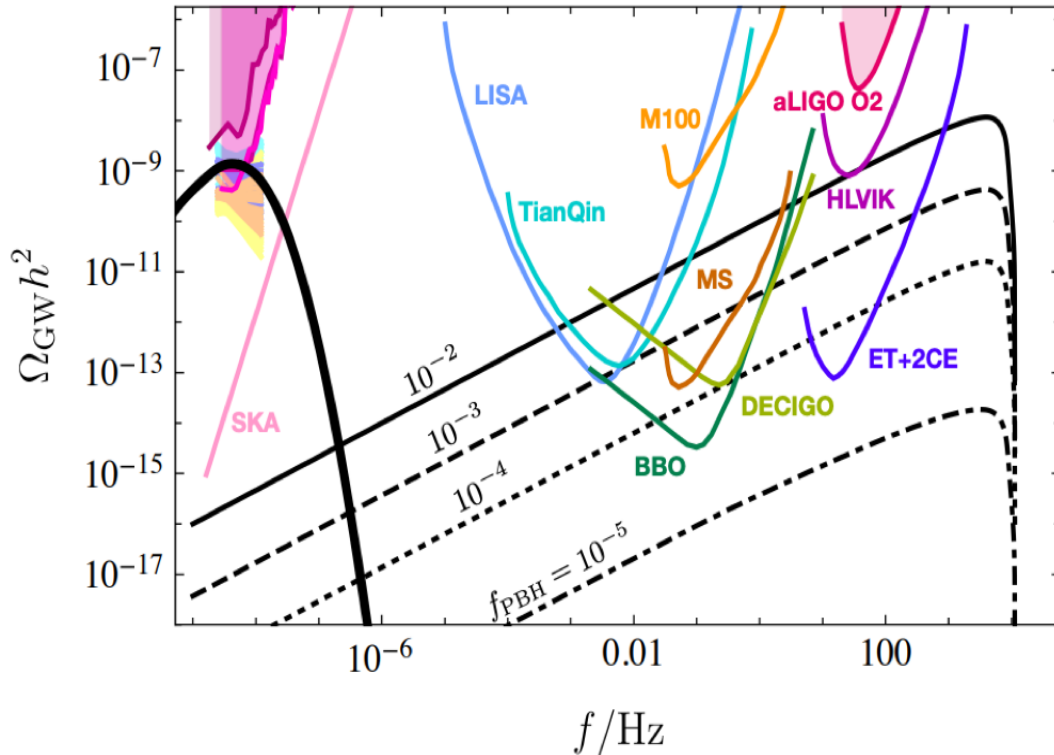
Cosmic string network for the different realization of parameter $G\mu$ with $\alpha = 0.1$.



Y Cui et al., JHEP 81, 2019

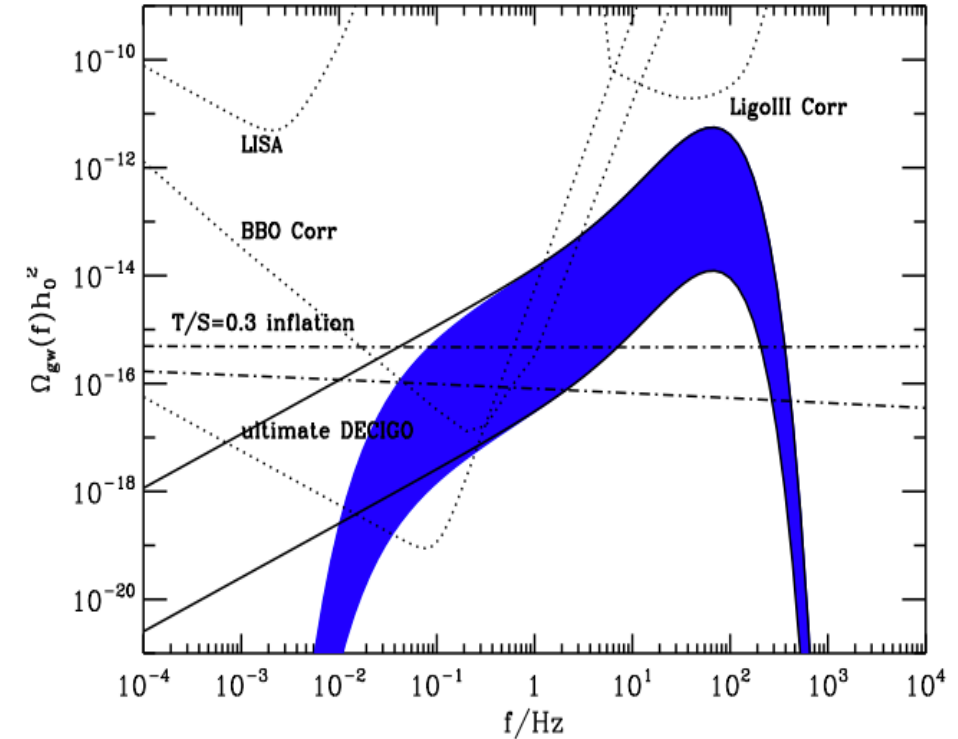
Cosmological backgrounds

PBHs. Solid black line for PBHs with one solar mass and various realizations of energy densities.



Kohri and Terada, PLB 813 (136040) 2021

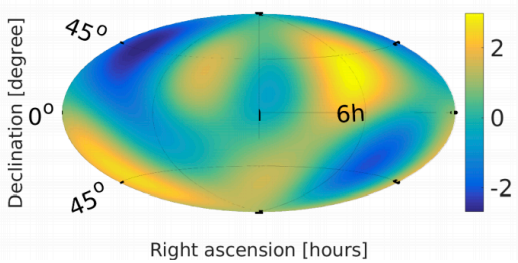
Pop III core collapse SNe.



A. Buonanno et al., PRD 72(084001)2005

Stochastic background

- An incoherent superposition of a large number of sources defined by statistical properties, isotropic, unpolarized, stationary and Gaussian.

Background	Astrophysical origin	Cosmological origin
<p>GW radiation</p> 	<p>Unresolved GW source Background.</p> <p>Foreground for cosmological signal searches.</p>	<p>GW signal from primordial universe.</p>

Why stochastic background?

- A GW stochastic background may be the next class of GW signals to be detected.
- Statistical detection whose confidence level will grow with the observation time.

$$\Omega_{GW}(f) = \frac{1}{\rho_c} \frac{d\rho_{GW}}{d \ln f} \quad , \quad \rho_c = \frac{3 c^2 H_0^2}{8\pi G} \quad (2)$$

- To detect a primordial or early universe GW signal, with 3G detectors we have to reduce the foreground generated by $10^5 - 10^6$ mergers (NS-NS, BH-BH, NS-BH and other sources) in the universe per year.
- CBC foreground of data stream has amplitude much higher than the detector noise which in turn is greater than the stochastic cosmological signal.
- To detect the primordial/cosmological signal, we have to understand the foreground, i.e., analyse signals using data from a detector network, reduce the GW merger foreground, subtract all the known binaries from the data stream.

Detecting SGWB with 3G detectors

- Studied a subtraction-noise projection method to deal with astrophysical foreground.
- Based on a geometrical interpretation of matched filtering.
- Allows to access the weak signals like a stochastic GW background, irrespective of the residual noise in the data.
- Required methods are :
 - Parameter estimation of detected binary signals.
 - Reduce contributions from binary signals as much as necessary (subtraction, projection).
 - Implementing methods for stochastic signal search.

Sharma & Harms PRD **102**, 063009 (2020)

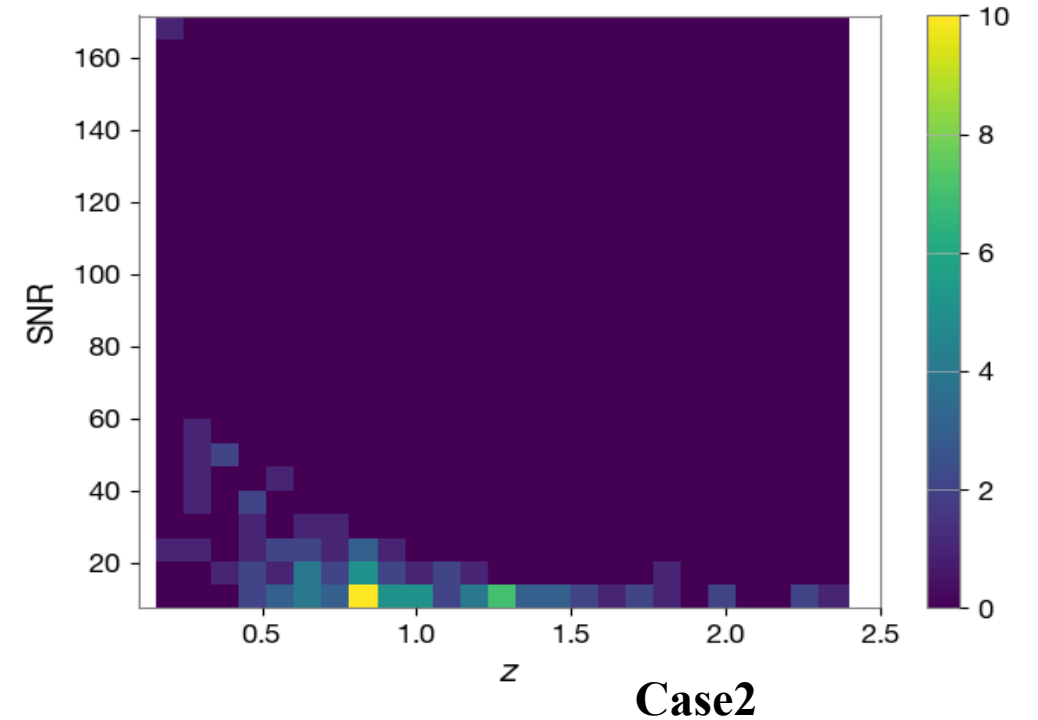
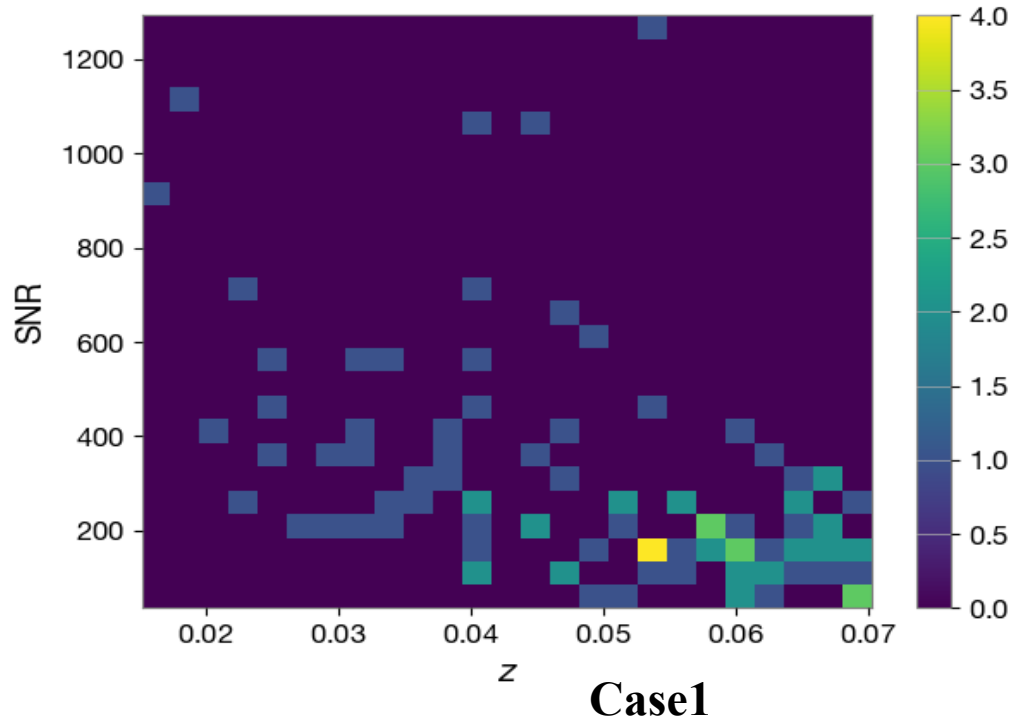
Jan Harms et al., PRD 77, 123010 (2008)

- Bilby for PE, a Python based Bayesian inference library for gravitational wave astronomy.
- Using uniform priors, calculated the maximum likelihood parameters.

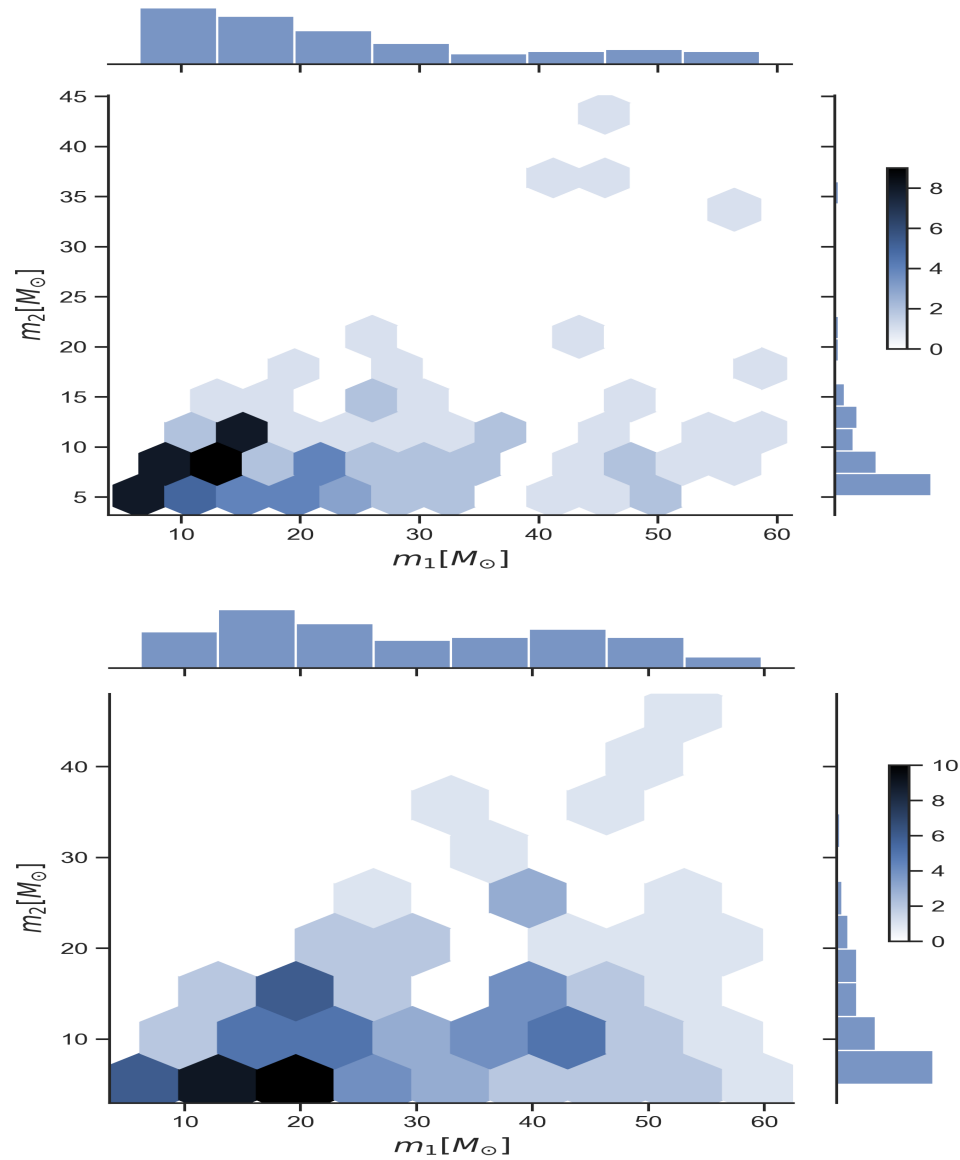
Gregory Ashton *et al* *ApJS* **241** (2019) 27

Simulation overview

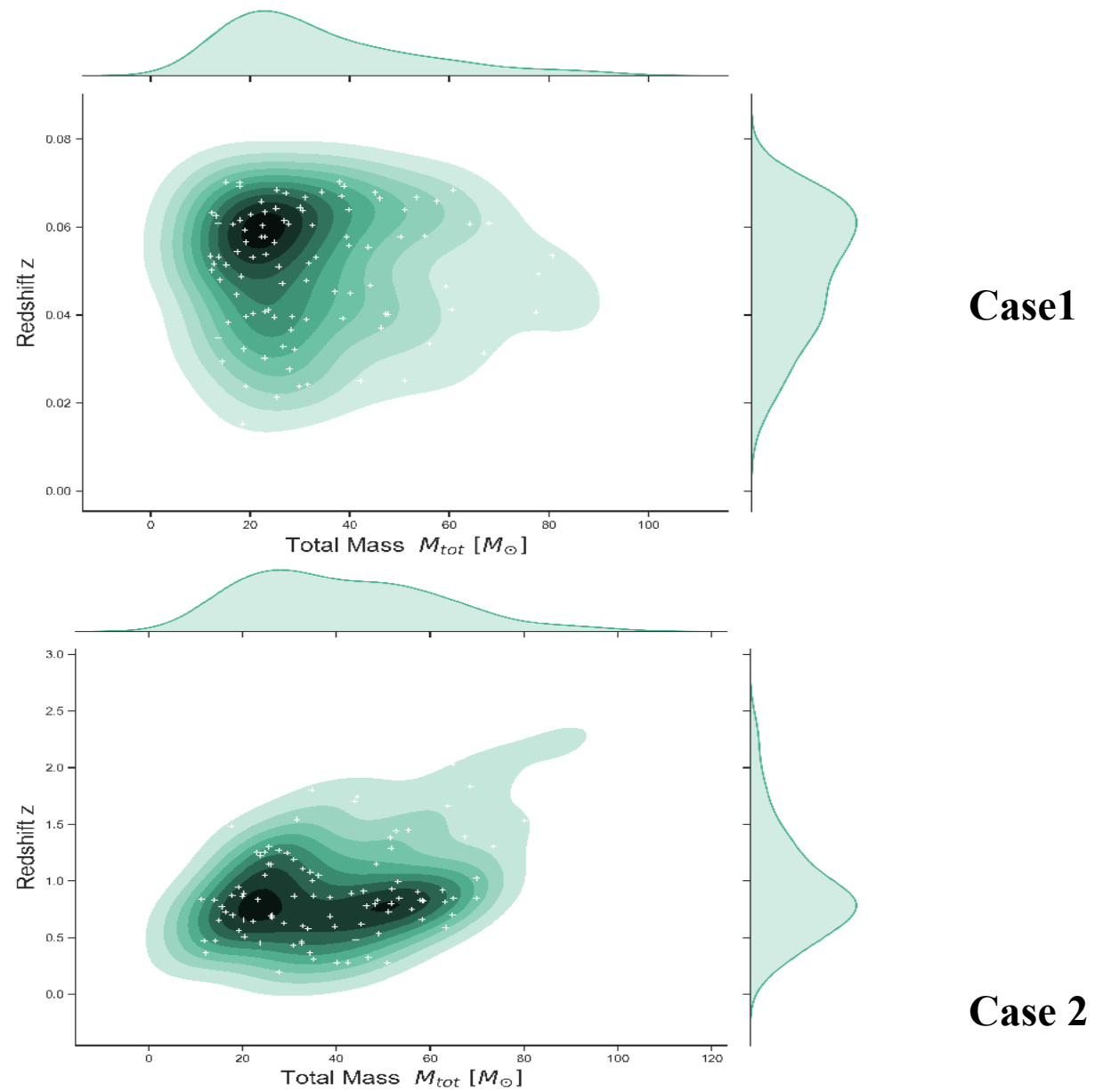
- Case studies
 - **Case1:** Highest SNR BBH signals (all BBHs are in local Universe with redshift $z < 0.1$).
 - **Case2:** BBH signals with $\text{SNR} > 10$.
 - **Case3:** BBHs with $\text{SNR} < 10$ (under study).
- These case studies depend upon the choice of BBH redshift distribution.



Distribution of BBHs



01/02/21



Total mass vs Redshift distribution of BBHs

Simulation overview

- Simulation of data
 - Performing the Bayesian parameter estimation to estimate the best-fit waveform of injected BBH signals.
 - These 100 BBH signals are generated using “IMRPhenomPv2” waveform.
 - **Injections:** 1.3-year-long stretch of GW data for ET and CE detectors divided into 10000 time segments of length 4096 s.
 - The 100 BBH signals are injected with random time shift such that phase relations between all signals are randomized.
 - **Subtraction:** Estimated best-fit waveforms are then subtracted from the data to reduce the foreground contribution toward stochastic searches.
 - **Projections:** Residual noise data due to mismatch between true and estimated best-fit waveform. Using Fisher matrix to project out the residual noise data.
 - Since projection requires Fisher matrices and derivatives of waveform with respect to BBH parameters, a differential numerical approach is followed for the purpose.
 - Cross-power spectral densities of time series between all detector pairs are calculated.
 - Optimal filters are used to evaluate the ultimate sensitivity of the network to an SGWB.

Cross-correlation between detectors

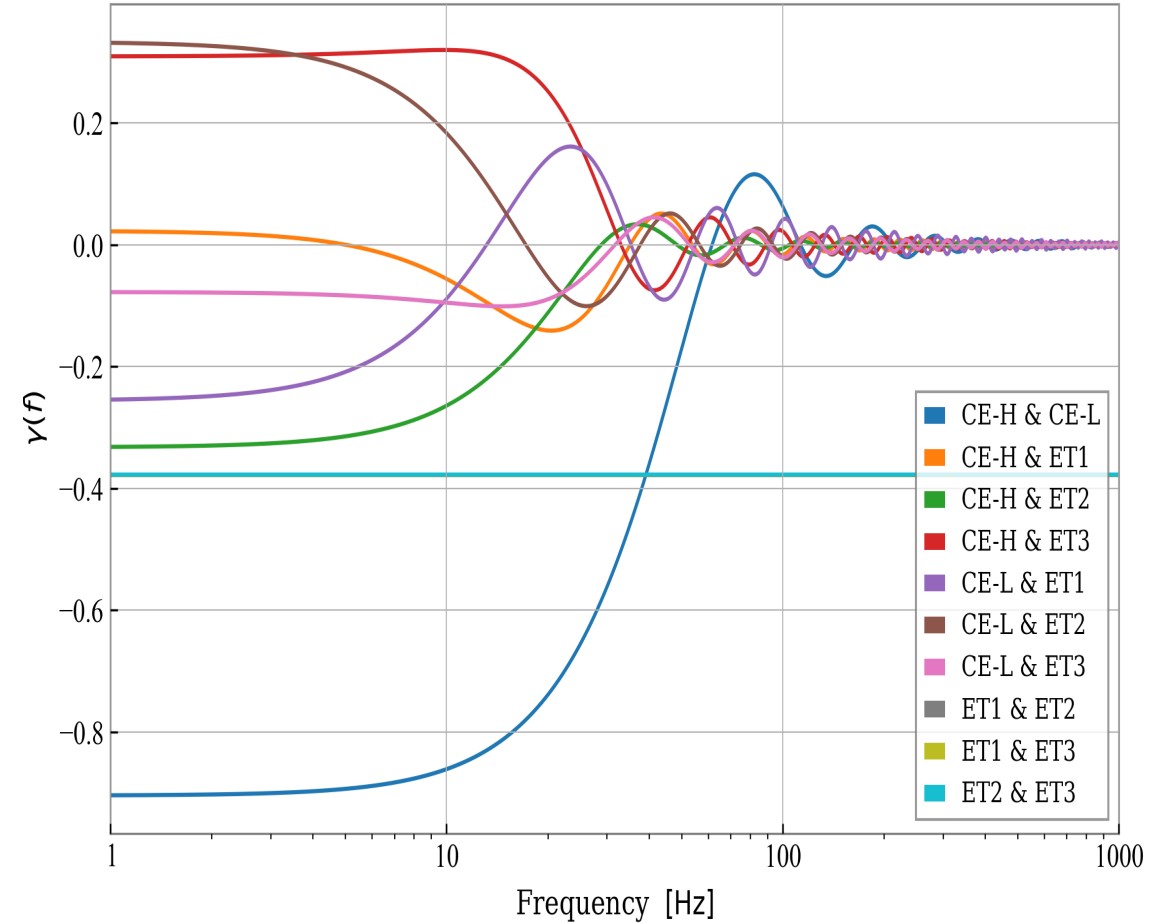
- The cross-power spectral densities between two detectors due to SGWB is

$$C_{IJ}(f) = S_{GW}(f)\gamma_{IJ}(f) \quad (3)$$

where $\gamma_{IJ}(f)$ is overlap reduction function and

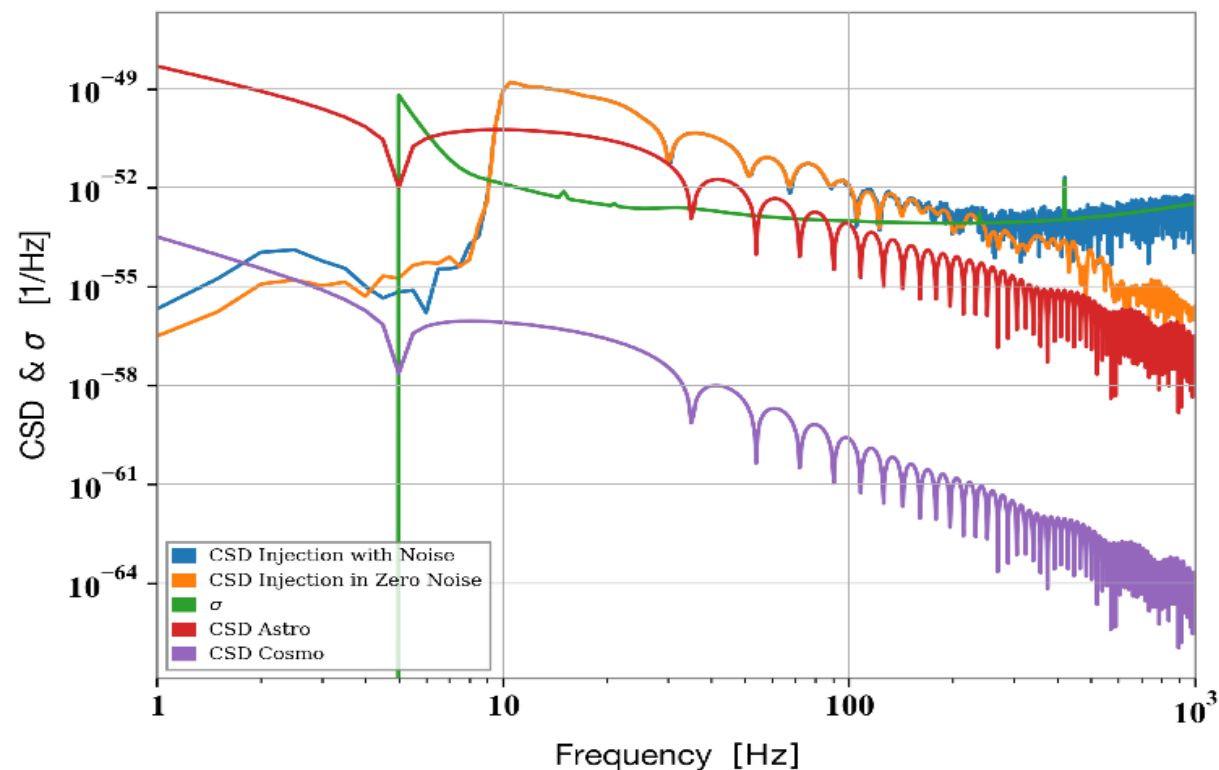
$$S_{GW}(f) = \frac{3H_0^2}{10\pi^2} \cdot \frac{\Omega_{GW}(f)}{f^3} \quad (4)$$

$$\Omega_{GW}(f) = \begin{cases} 7 \times 10^{-10} \times \left(\frac{f}{10 \text{ Hz}}\right)^{\frac{2}{3}}, & \text{astro SGWB} \\ 10^{-15}, & \text{cosmo SGWB} \end{cases}$$

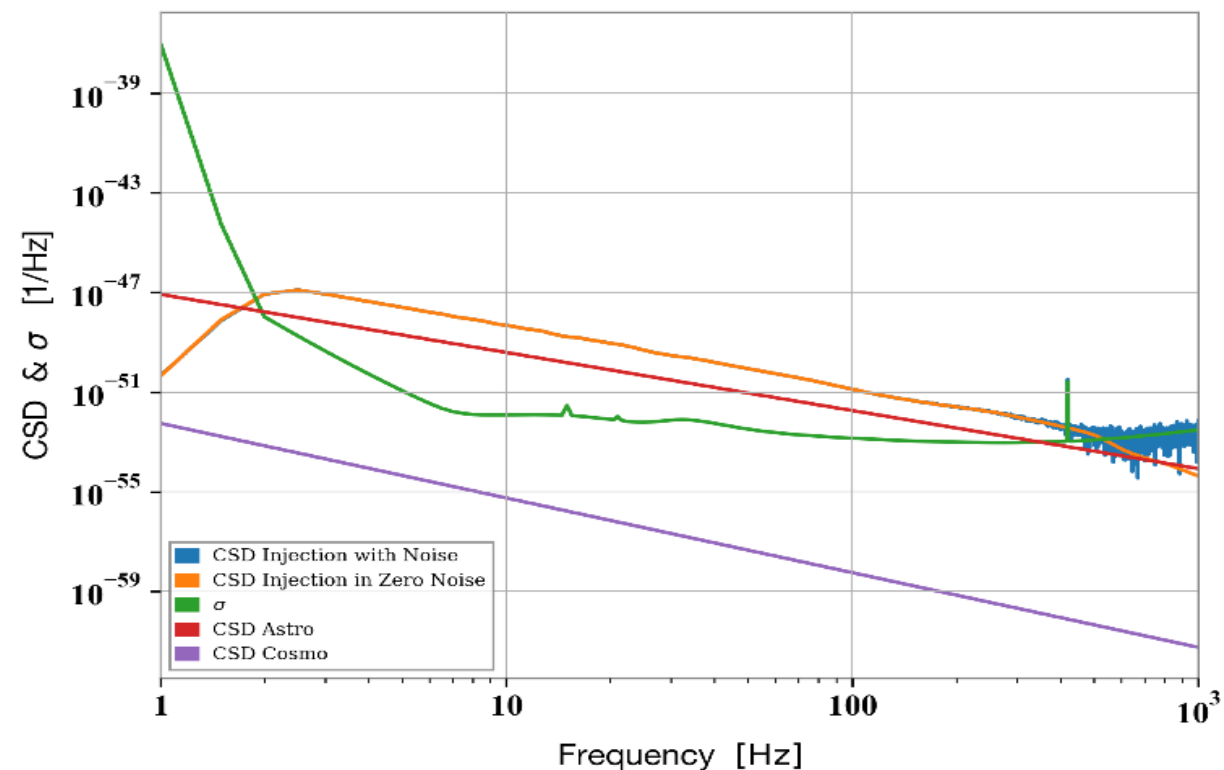


Injected astrophysical background

CSD plot after injecting BBH signals into detector network with and without instrumental noise. The plot is shown for the detector pair formed by CE and one of the interferometers of ET.



CSD between ET interferometers with injected BBHs with and without instrumental noise. The plot is shown for the complete ET detector, averaged over the three individual detectors of ET.



Matched filtering and Fisher matrix

- For a Gaussian instrumental noise, the metric of statistical manifold is

$$\Gamma_{\alpha\beta} = \langle \partial_\alpha h(\vec{\lambda}) | \partial_\beta h(\vec{\lambda}) \rangle \quad (5)$$

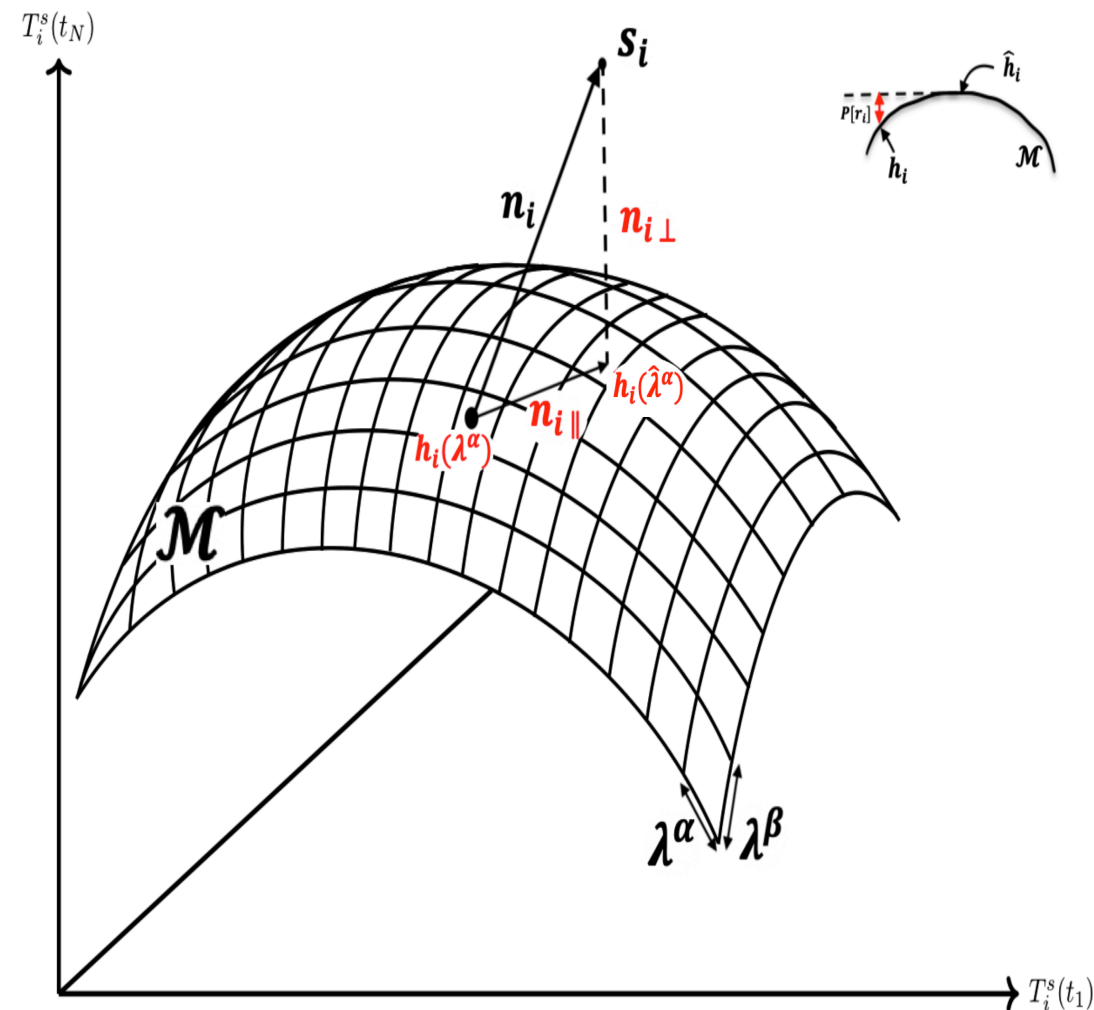
$$\Gamma_{\alpha\beta} = 4 \int_0^\infty df \frac{\text{Re} \left(\partial_\alpha h(\vec{\lambda})(f) \partial_\beta h(\vec{\lambda})^*(f) \right)}{S_n(f)} \quad (6)$$

- For a GW detector to measure output s , Gaussian probability density is

$$p(n = n_0) \propto e^{-\frac{\langle s - h | s - h \rangle}{2}} \quad (7)$$

- If best-fit waveform \hat{h} , maximises the likelihood, it must fulfil

$$\langle s - \hat{h} | \partial_\alpha \hat{h} \rangle = \langle n + (h - \hat{h}) | \partial_\alpha \hat{h} \rangle = 0 \quad (8)$$



Sources of confusion noise

- What can contribute to the confusion noise in 3G detectors?
 - Confusion noise due to binaries, i.e. overlapping in binary signals, unresolved binaries.
 - Noise due to resolved binaries, i.e. residual noise.

Overlapping in binary signals

- BBH signal in ET and CE can contribute to overlap between various signals.

$$s(t) = n(t) + \sum_j h_j(t) \quad (9)$$

- Optimal matched filtering of data for signal $h_k(t)$ is

$$\langle s | h_k \rangle = \langle n | h_k \rangle + \sum_{j \neq k} \langle h_j | h_k \rangle + \langle h_k | h_k \rangle \quad (9)$$

- In ET, BBH signals will rarely have significant overlap.

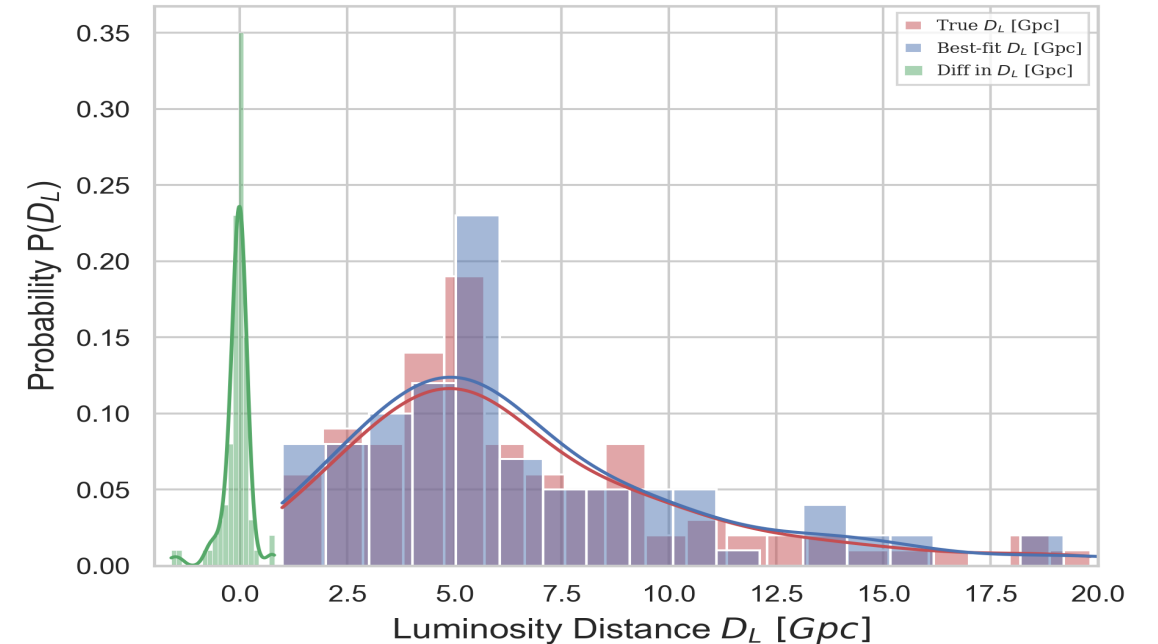
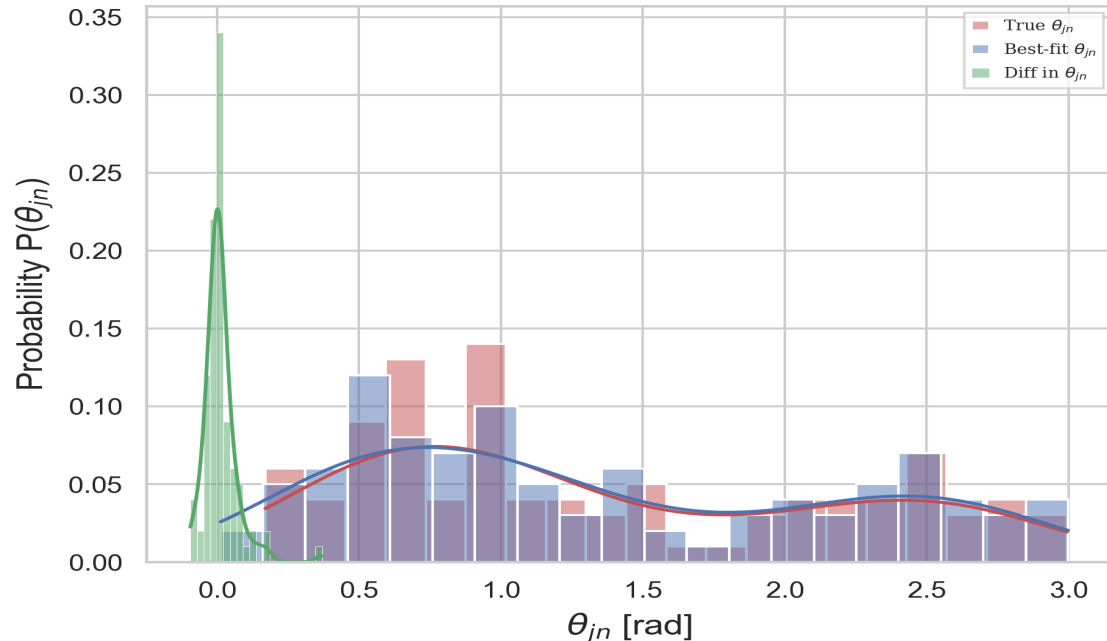
Subtraction of best-fit waveforms

- The mis-match between the true and estimated best fit parameter values

$$\delta\lambda^\alpha = \hat{\lambda}^\alpha - \lambda^\alpha \propto \frac{1}{SNR} \quad (11)$$

$$\delta\lambda^\alpha = \delta_n\lambda^\alpha + \delta_{temp}\lambda^\alpha \quad (12)$$

- The mis-match between the true source parameters and best-fit estimated parameters for simulated BBH parameters.



Subtraction cont...

- Estimated best-fit waveform will differ from true waveform

$$\delta h = \hat{h} - h = \partial_\alpha h \delta \lambda^\alpha + \mathcal{O}(\delta \lambda)^2 \quad (13)$$

- The norm-squared subtraction residual averaged over detector noise realization

$$\overline{\langle \delta h | \delta h \rangle} = \langle \partial_\alpha h | \partial_\beta h \rangle \overline{\delta \lambda^\alpha \delta \lambda^\beta} = \Gamma_{\alpha\beta} \Gamma^{\alpha\beta} = N_p \quad (14)$$

- Since $SNR = \sqrt{\langle h | h \rangle}$, amplitude of signal after subtraction

$$\frac{\delta h}{h} = \frac{\sqrt{N_p}}{SNR} \quad (15)$$

- After the subtraction of best-fit waveforms, we are left with residual noise + instrumental noise.

Subtraction cont...

- Mean square of instrumental noise

$$\overline{\langle n|n \rangle} = 2f_{max}T_{obs} \quad (16)$$

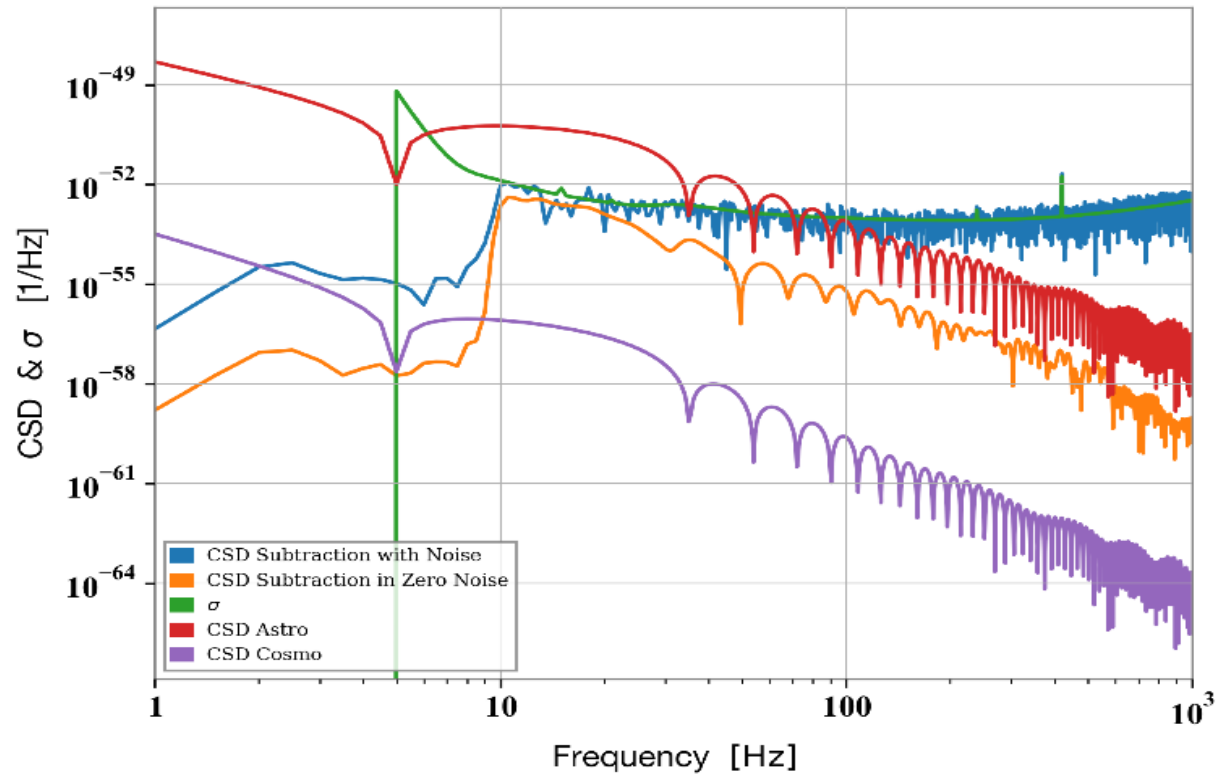
- Post-subtraction, data are

$$\begin{aligned} \overline{\langle s - \hat{h} | s - \hat{h} \rangle} &= \overline{\langle n + h - \hat{h} | n + h - \hat{h} \rangle} = \overline{\langle n - \delta h | n - \delta h \rangle} \\ &= \overline{\langle n_{\perp} + n_{\parallel} - \delta h | n_{\perp} + n_{\parallel} - \delta h \rangle} = \overline{\langle n_{\perp} | n_{\perp} \rangle} \\ &= 2f_{max}T_{obs} - N_P \end{aligned} \quad (17)$$

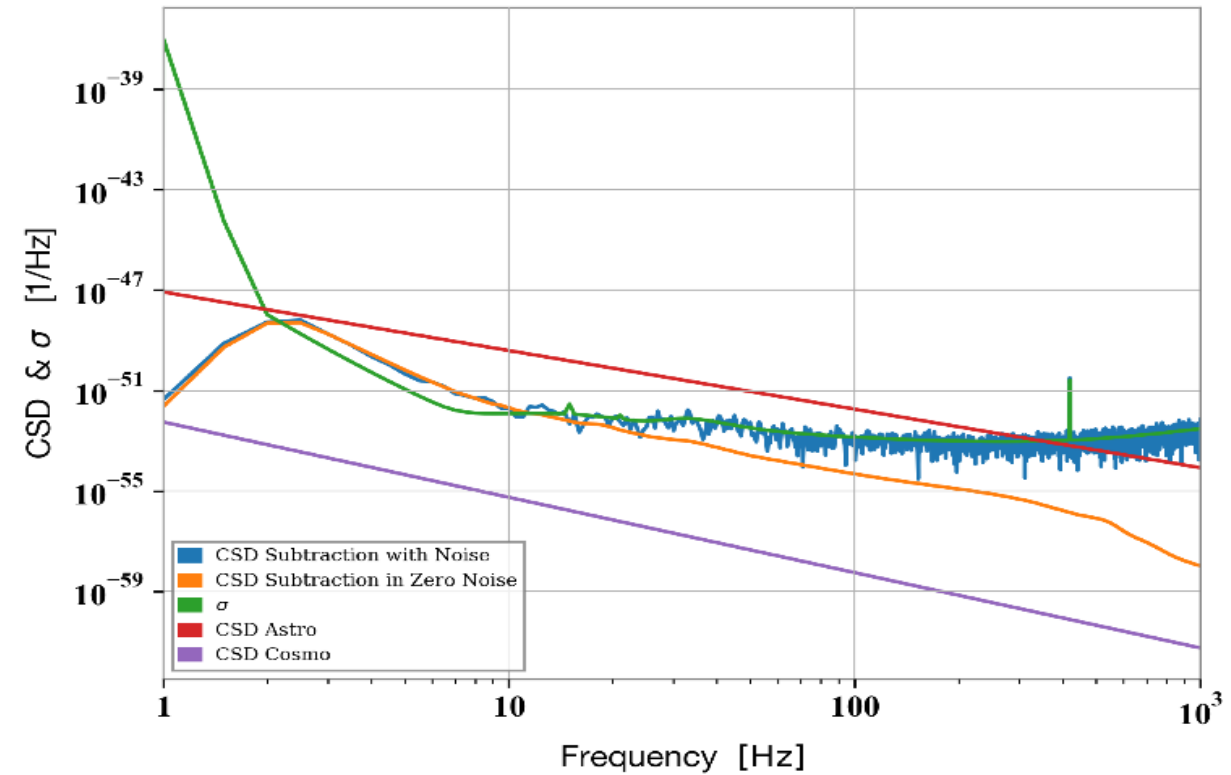
- Reduces the signal spectral density by a factor of $\frac{1}{SNR^2}$.
- Subtraction of best fit causes a reduction in the norm-squared of data.
- Subtraction removes part of noise in addition to the signal.
- This small piece of noise is responsible for the parameter estimation errors.

Subtracted astrophysical background

CSD plot after subtracting estimated best-fit BBH signals from the detector network with and without instrumental noise. The plot is shown for the detector pair CE and ET.



CSD plot after subtraction of best-fit estimated BBH signals with and without instrumental noise. The plot is shown for the complete ET detector, averaged over the three individual detectors of ET.



Projection of subtraction residuals

- The residual errors after subtracting the best-fit waveforms are

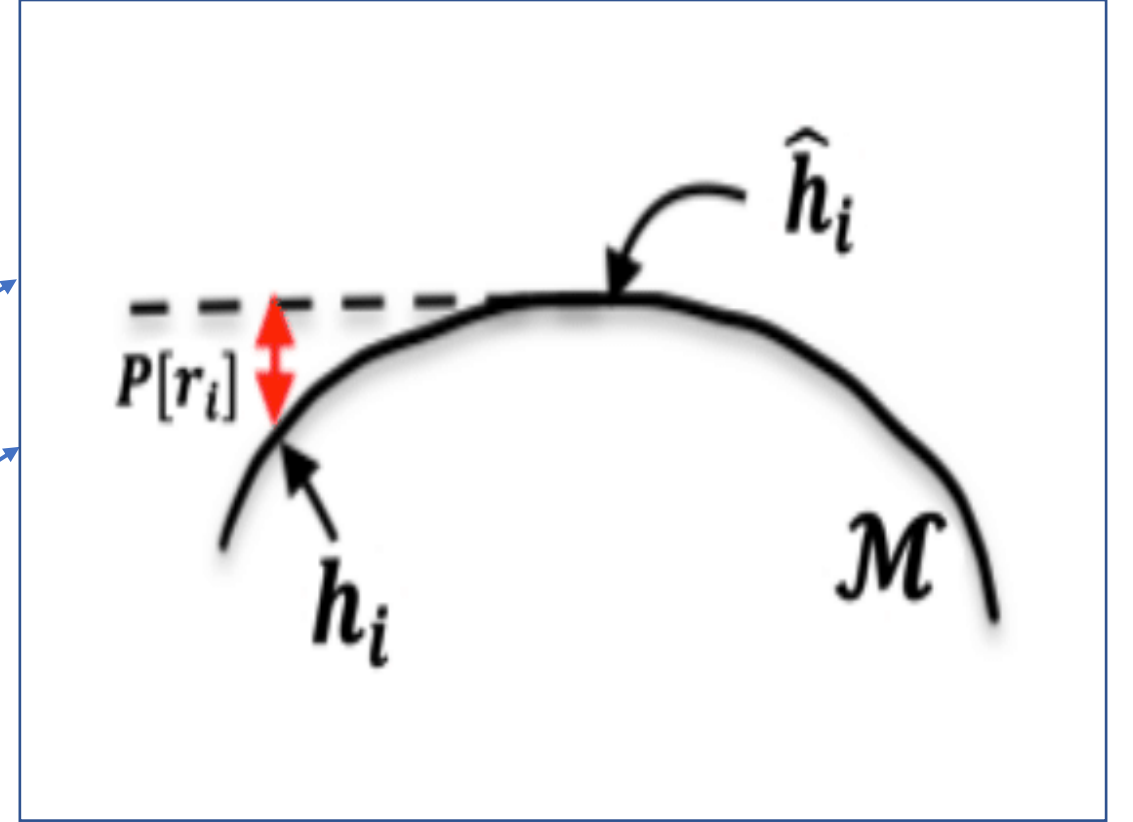
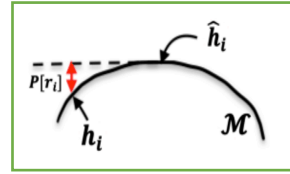
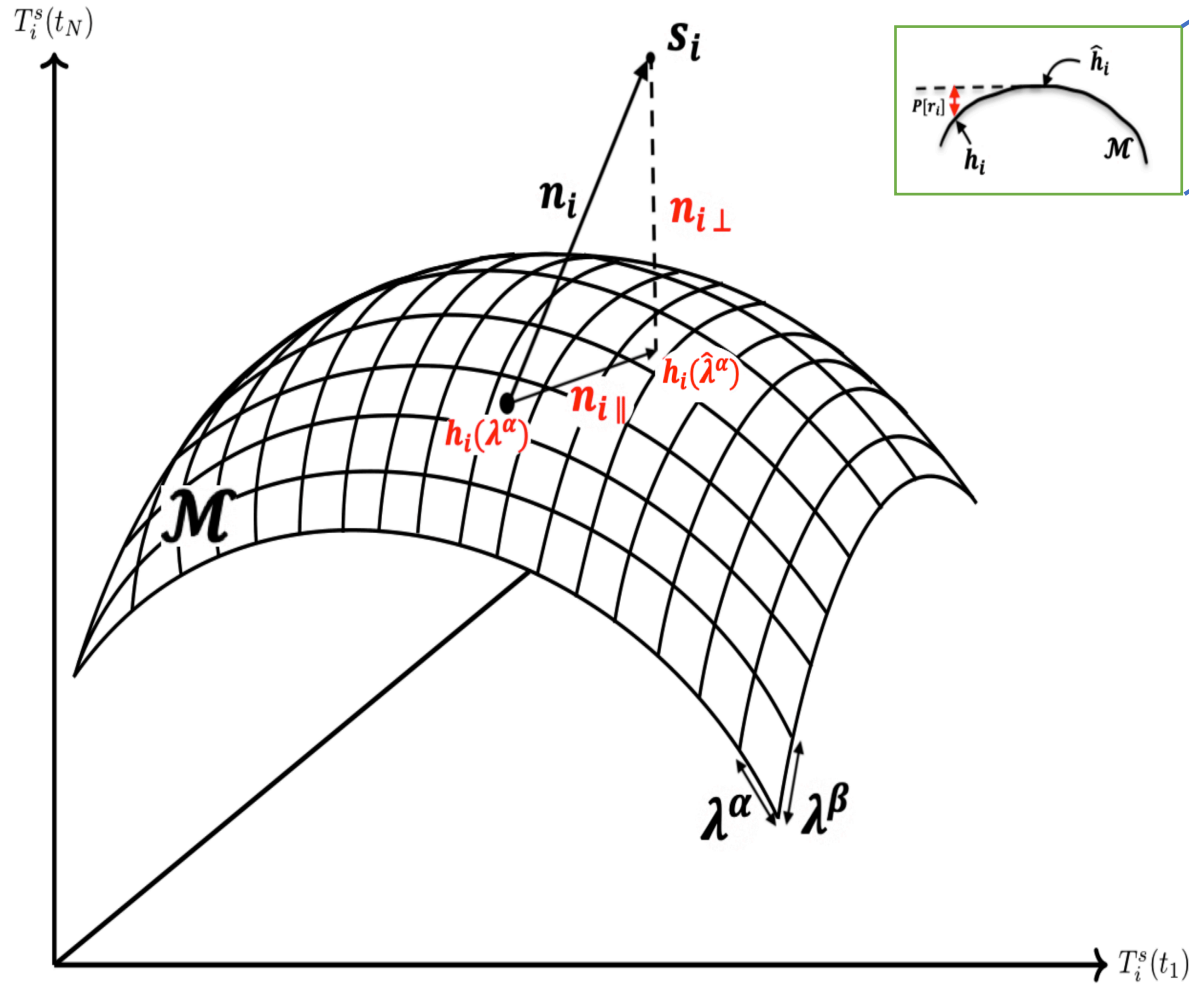
$$\delta H(t) = \partial_\alpha H(t) \delta \lambda^\alpha + \frac{1}{2} \partial_\alpha \partial_\beta H(t) \delta \lambda^\alpha \delta \lambda^\beta \quad , \quad \alpha, \beta = 1, 2 \dots N_P \quad (18)$$

- Projection operator which will eliminate the residuals $r = s - \hat{h}$ is

$$P = 1 - \Gamma^{\alpha\beta} |\partial_\alpha H\rangle \langle \partial_\beta H| \quad (19)$$

- Projecting the residual data from the detector

$$P[r_i](t) = r_i(t) - \Gamma_i^{\alpha\beta} \langle \partial_\beta \hat{h}_i | r_i \rangle \partial_\alpha \hat{h}_i(t) \quad (20)$$



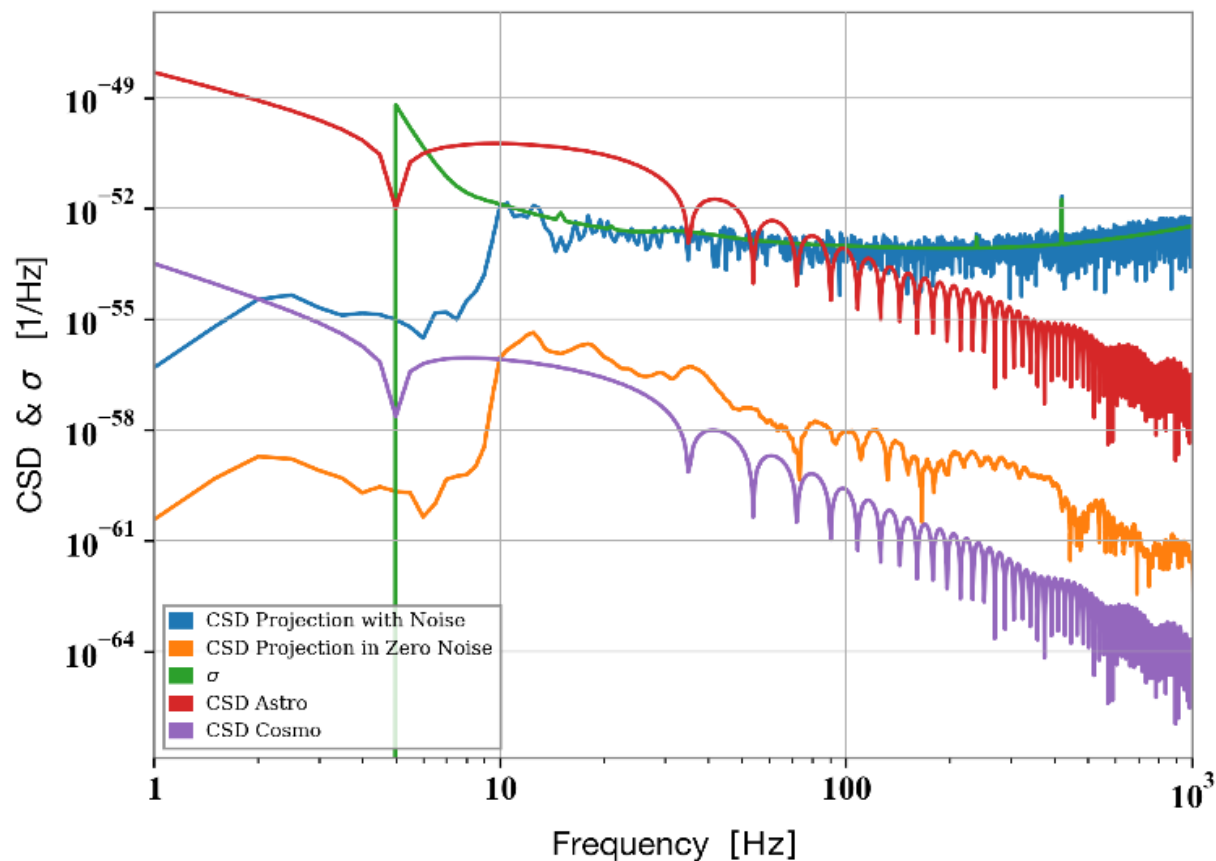
- Quantity remained after the projection of residuals

$$P[r_i] = n_{i\perp} + b_{i\perp} + \mathcal{O}\left(\frac{h_i}{SNR^2}\right) \quad (21)$$

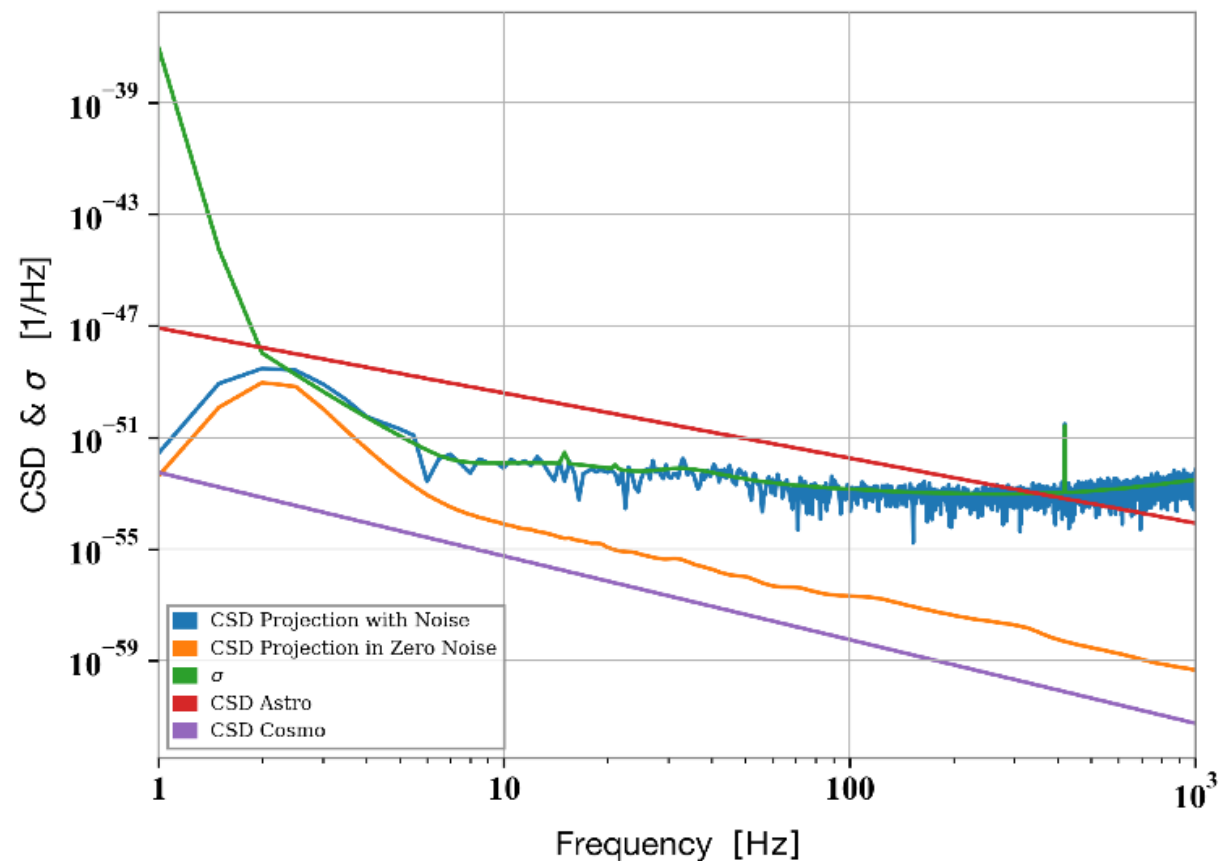
Projection of residuals

Sharma & Harms, manuscript in prep.

CSD plot after the projection of subtraction residuals, shown for CE and ET-D_1 detector network.

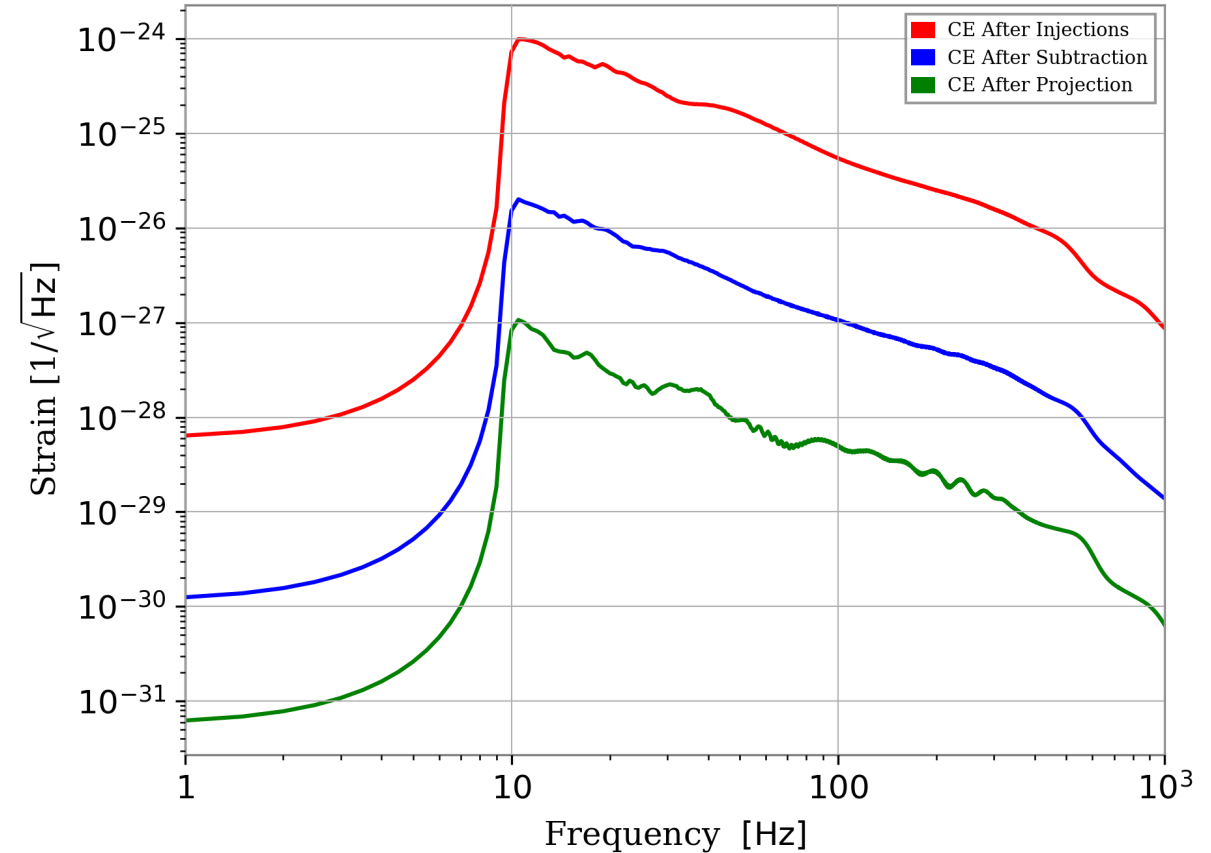
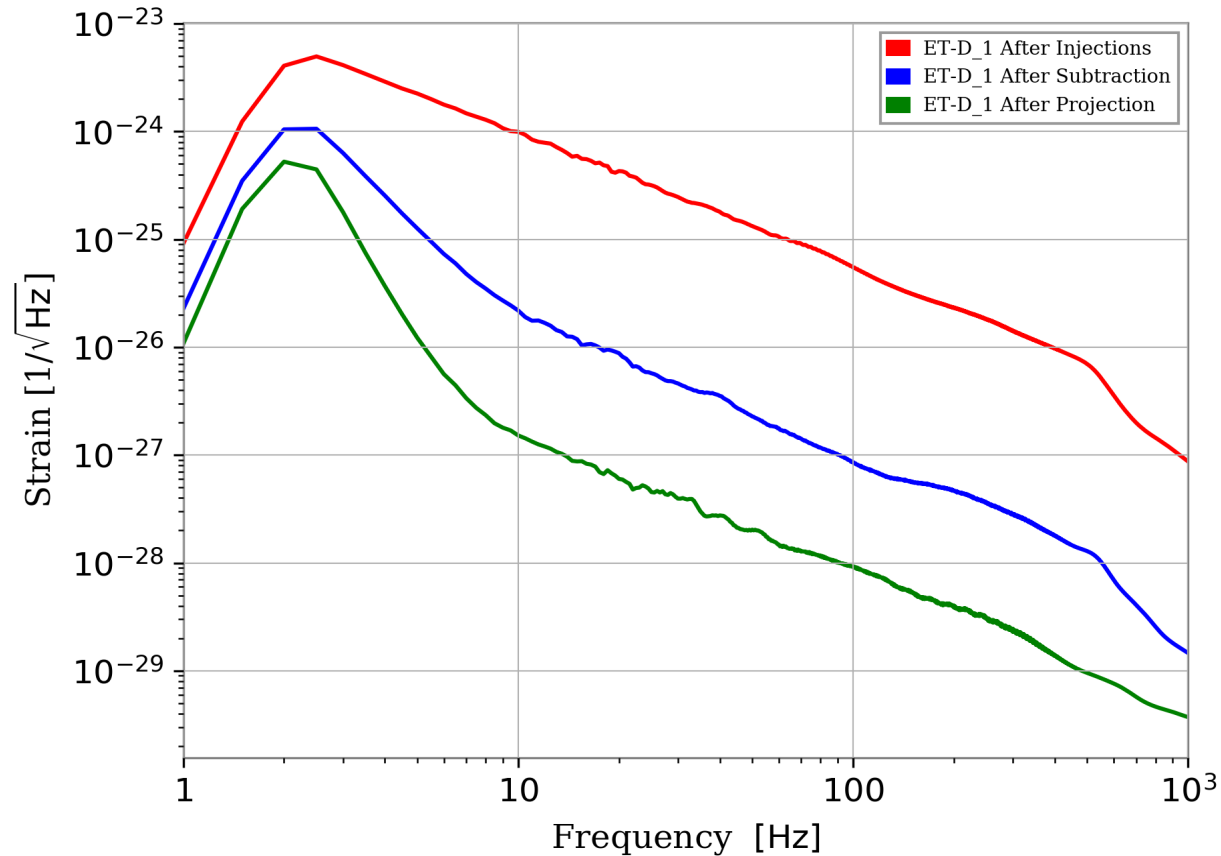


CSD plot after the projection of subtraction residuals, shown for averaged ET detector.

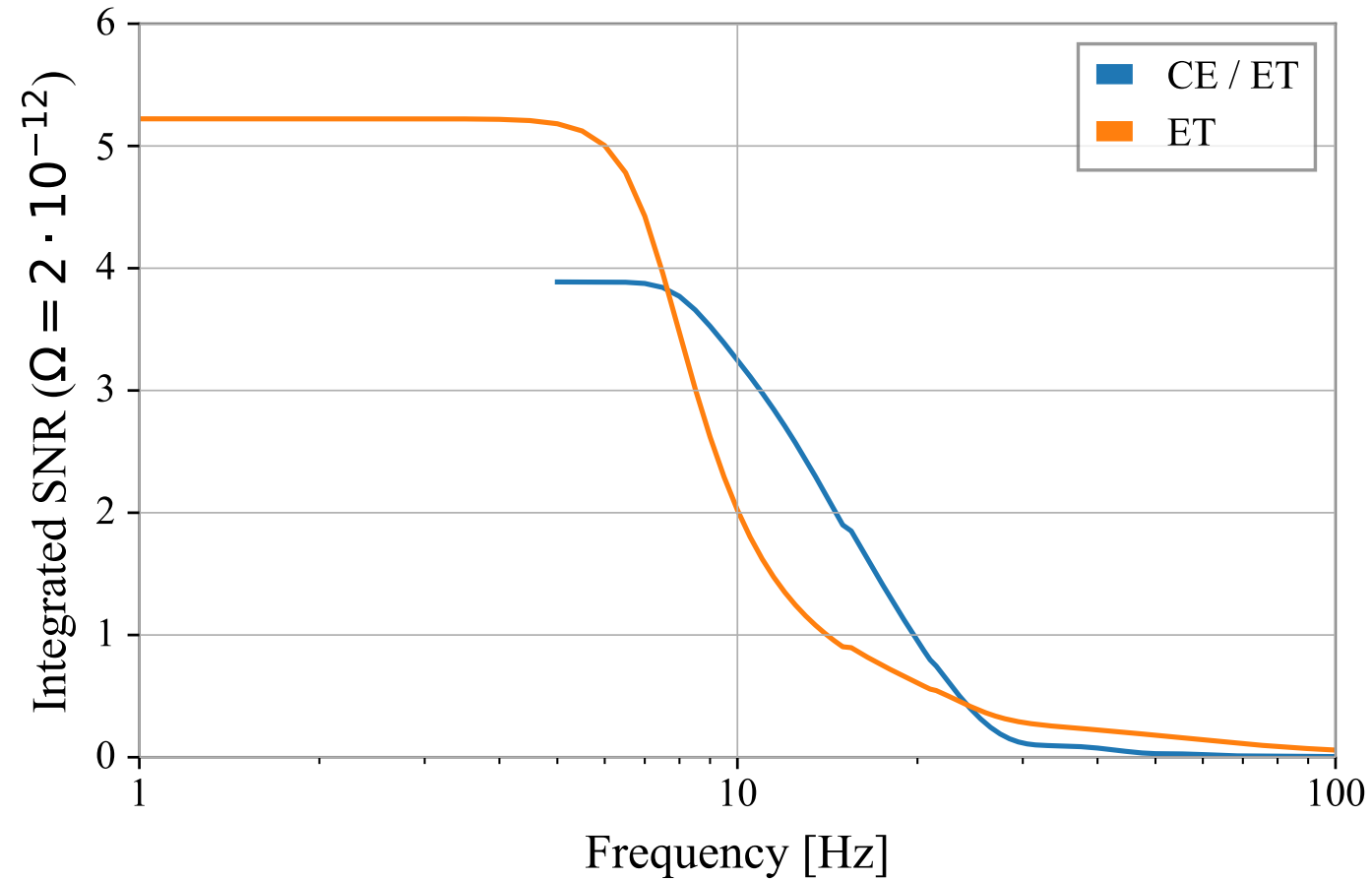


Spectrum after Injection, Subtraction and Projection

- Simulated spectrum (i.e. sqrt of PSDs) of astrophysical foreground after injecting 10^6 BBH signals, subtraction residual spectrum after the subtraction of best-fit signals and spectrum after projecting out the residuals are shown for ET and CE detector.



SNR of a SGWB search with ET and CE detectors



Work in progress...

- Understanding the implication and effectiveness of subtraction-noise projection method in low SNR regime.
- $\text{SNR} < 10$, $\text{SNR_threshold} < \text{SNR} < 10$.
- What would be the role of waveform models and associated systematics?
 - Parameter estimation of CBC.
 - If we use one waveform model to create astrophysical foreground.
 - Another waveform to subtract this foreground.
 - Contribution to residual noise.

O3 analysis and upper limits on Ω_{GW}

- Stochastic analysis is performed using O3 data from aLIGO and AdV detectors.
- aLIGO and AdV form three detector pairs: HL, HV and LV.
- The O3 data consist of two data sets O3a (first half) and O3b (second half), resulting in total of eleven months of data.

Data Set	Start Time	End Time
O3a	April 1 2019 UTC 15:00	October 1, 2019 UTC 15:00
O3b	November 1, 2019 UTC 15:00	March 27, 2020 UTC 15:00

- Stochastic analysis is first performed for each dataset and pair of detectors in the frequency range 20 – 1726 Hz and then combining them in an optimal way.

O3 analysis cont...

- To deal with non stationarity of the GW detector data, each detector pair data are divided into segments of 192 s.
- This provides us with a suitable frequency resolution to remove the sharp lines from the data.
- The data in each time segment then decimated from original sampling rate of 16384 Hz to 4096 Hz and high-pass filtered with 11 Hz corner frequency.
- Time segments are Hann-windowed with 50% overlap to recover SNR.
- Computed a discrete Fourier transform on each time segment resulting in a frequency resolution of $\Delta f = 1/32$ Hz.
- For a GW detector with N independent measurements, overall output is

$$s_i = h + n_i \quad i = 1, \dots, N \quad (22)$$

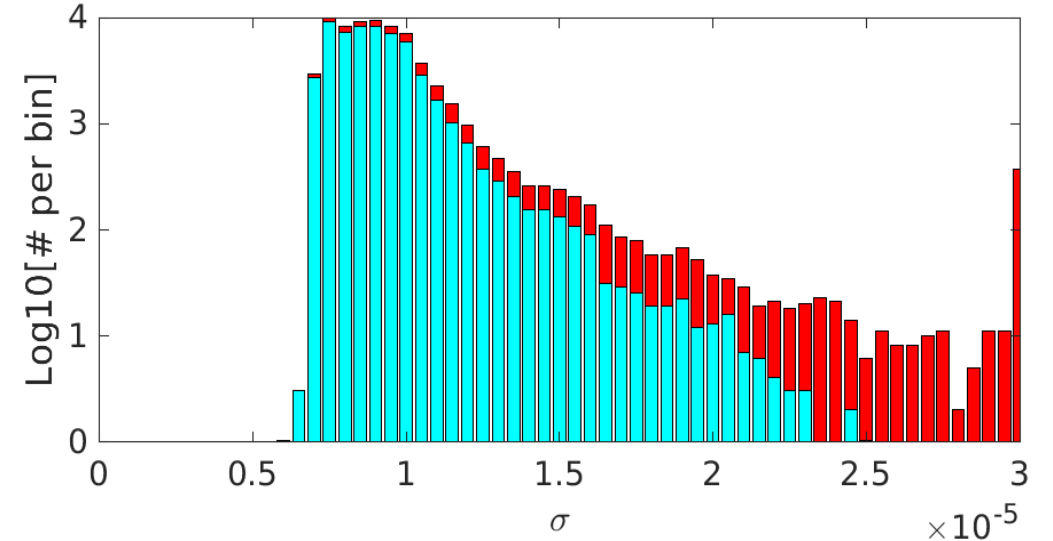
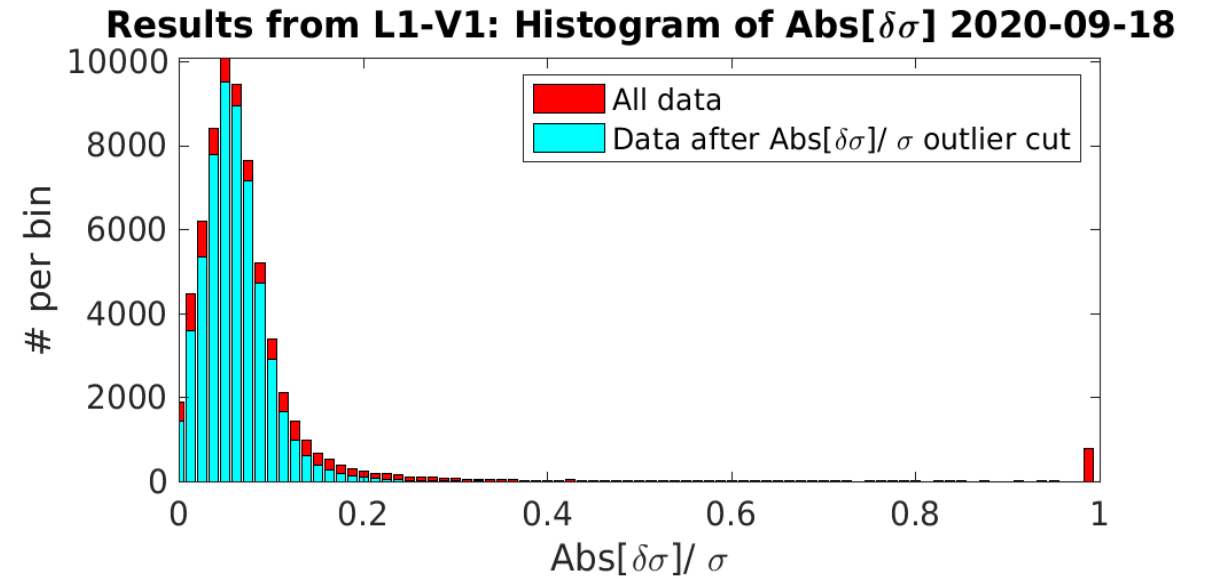
h is an SGWB and n is instrumental noise.

Data quality cuts

- Data quality cuts led to 50% of data loss in H and L detector pair due to higher rate of loud glitches.
- Data cuts or delta sigma cuts remove all the segments with

$$\delta\sigma = \frac{|\sigma - \sigma'|}{\sigma} > 0.2 \quad (23)$$

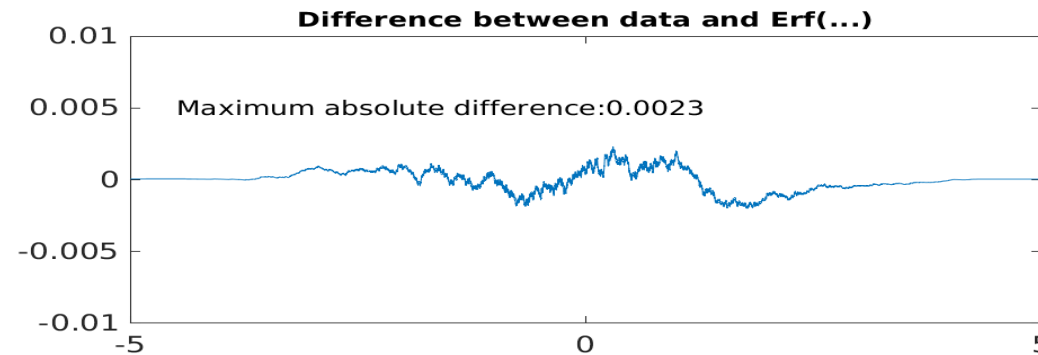
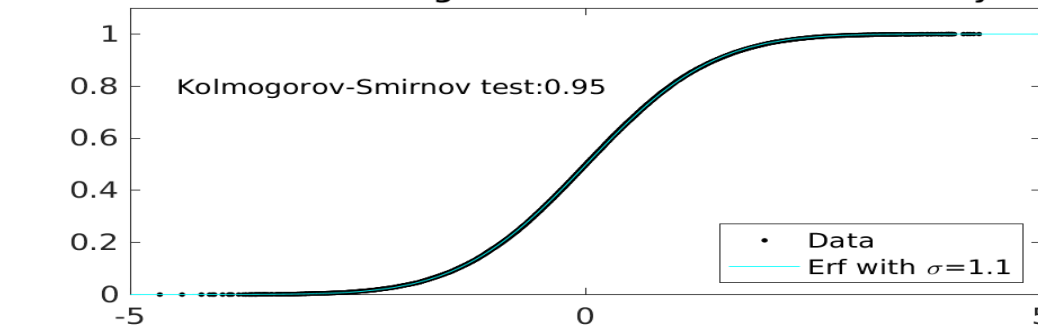
- Delta σ cuts remove the outliers from the excess residual noise distribution, making data more stationary.



Gaussianity of dataset after $\delta\sigma$ cuts

- Gaussian nature of data after performing $\delta\sigma$ cuts was cross-checked by using Kolmogorov-Smirnov test for each detector pair.

Results from L1-V1: Kolmogorov-Smirnov test for Gaussianity 2020-09-1



Coherence between the detector pairs

- To identify and eliminate all contaminated frequency bins.
- Coherence for a detector pair is

$$\xi(f) = \frac{|\langle P_{IJ}(f) \rangle|^2}{\langle P_I(f) \rangle \langle P_J(f) \rangle} \quad (24)$$

- Coherence reveals several correlated frequency lines for each detector pair.
- Notch frequencies witnessed in each detector pair during the analysis were excluded from the data.

Baseline	Frequencies (Hz)
HL	20.21875, 20.25, 20.34375, 174.5625, 331.90625, 409.9375, 410.3125, 434.90625, 1083.6875, 1083.09375
HV	26.1875, 46-51, 87.09375, 331.90625, 410.3125, 1083.6875
LV	46-51, 71.25, 434.90625, 1083.09375

- 46-51 Hz frequency lines observed in AdV are due to the active damping mechanical modes.

Cross-correlating the data between detector pairs

- For a stationary, Gaussian, unpolarized and isotropic SGWB, cross-correlation in each frequency bin of the data is

$$\hat{C}_{IJ}(f) = \frac{2}{T} \frac{\Re[\tilde{s}_I^*(f) \tilde{s}_J(f)]}{\gamma_{IJ}(f) S_{GW}(f)} \quad (25)$$

- Eq.(25) is normalized such that $\langle \hat{C} \rangle = \Omega_{GW}$. Thus the variance of $\hat{C}_{IJ}(f)$ is

$$\sigma_{IJ}^2(f) = \frac{1}{2T \Delta f} \frac{P_I(f) P_J(f)}{\gamma_{IJ}^2(f) S_{GW}^2(f)} \quad (26)$$

- The sum of all individual estimator in each frequency bin with a weighted average of cross-correlation across frequency bins f_k is

$$\hat{C}_{IJ} = \frac{\sum_k w(f_k) \hat{C}_{IJ}(f_k) \sigma_{IJ}^2(f_k)}{\sum_k w(f_k)^2 \sigma_{IJ}^{-2}(f_k)} \quad (27)$$

B. Abbott et al., PRD 100 (061101) 2019

cont...

$$\sigma_{IJ}^2 = \sum_k w(f_k)^2 \sigma_{IJ}^2(f_k) \quad (28)$$

with optimal weights for Ω_{GW}

$$w(f) = \frac{\Omega_{GW}(f)}{\Omega_{GW}(f_{ref})} \quad (29)$$

- Using

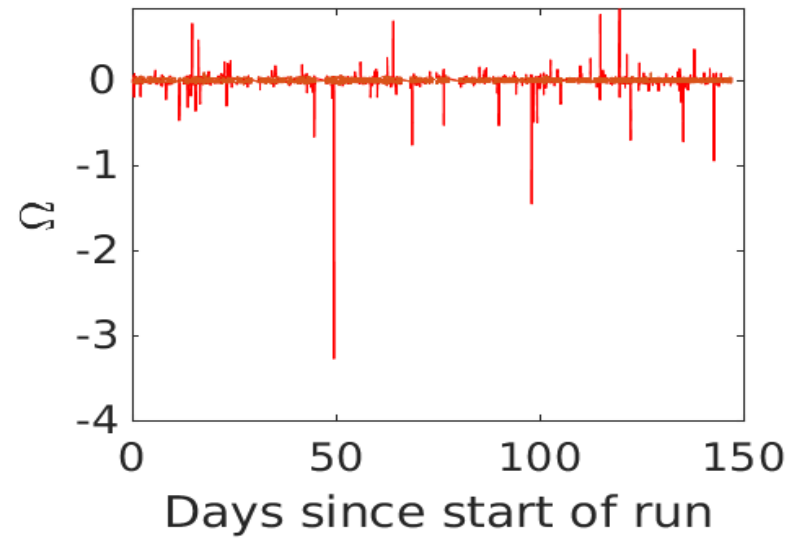
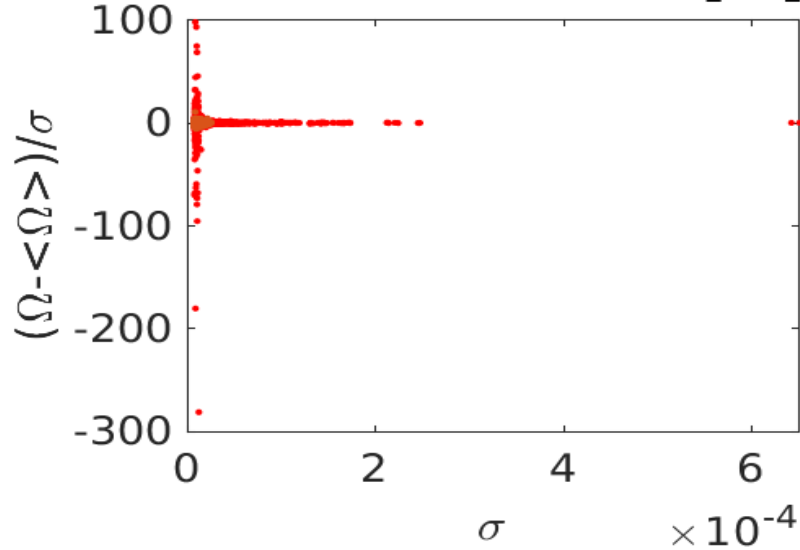
$$\Omega_{GW} = \Omega_{ref} \left(\frac{f}{f_{ref}} \right)^\alpha \quad (30)$$

stochastic pipe analysis can be applied to SGWB of any spectral shape. The most preferred values for power-law spectral index α , used in the stochastic analysis are $\alpha = 0, \frac{2}{3}, 3$.

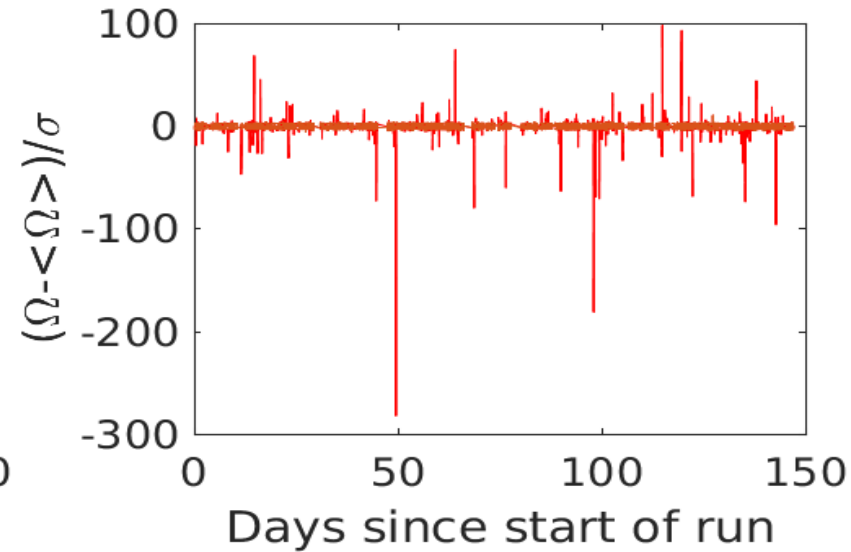
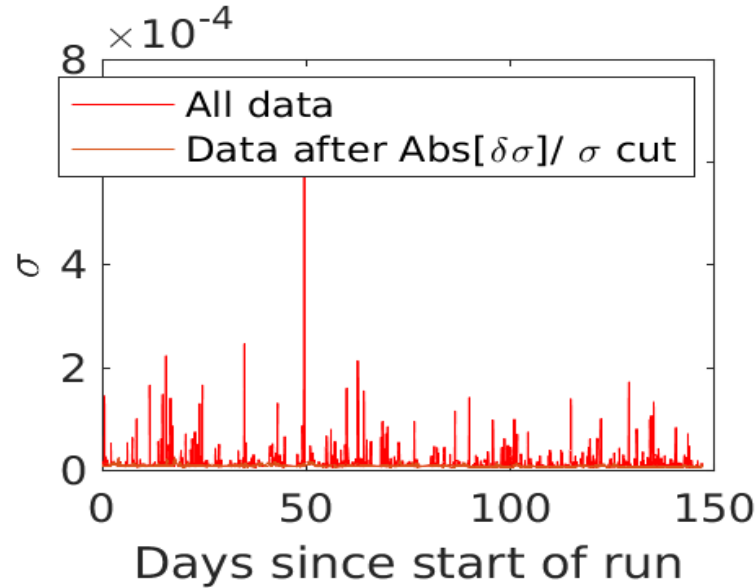
- The final optimal estimator for all detector pair is

$$\hat{C} = \frac{\sum_{IJ} \hat{C}_{IJ} \sigma_{IJ}^{-2}}{\sum_{IJ} \sigma_{IJ}^{-2}} \quad (31)$$

Results from L1-V1 for $\text{Abs}[\delta\sigma]/\sigma < \text{Inf} \times 10^{-3}$ 2020-09-18

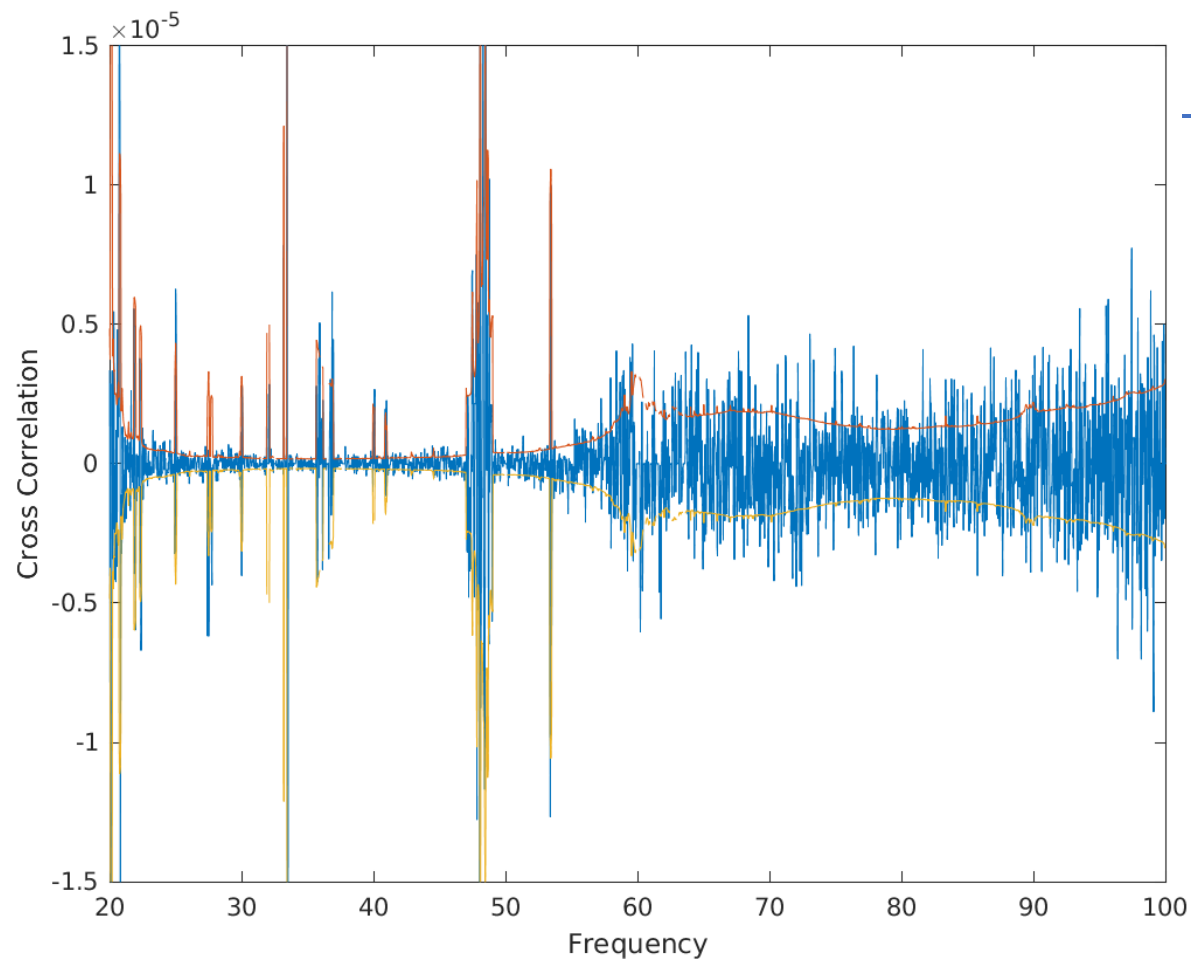


Plot showing the variation in Ω from the start of O3b analysis.

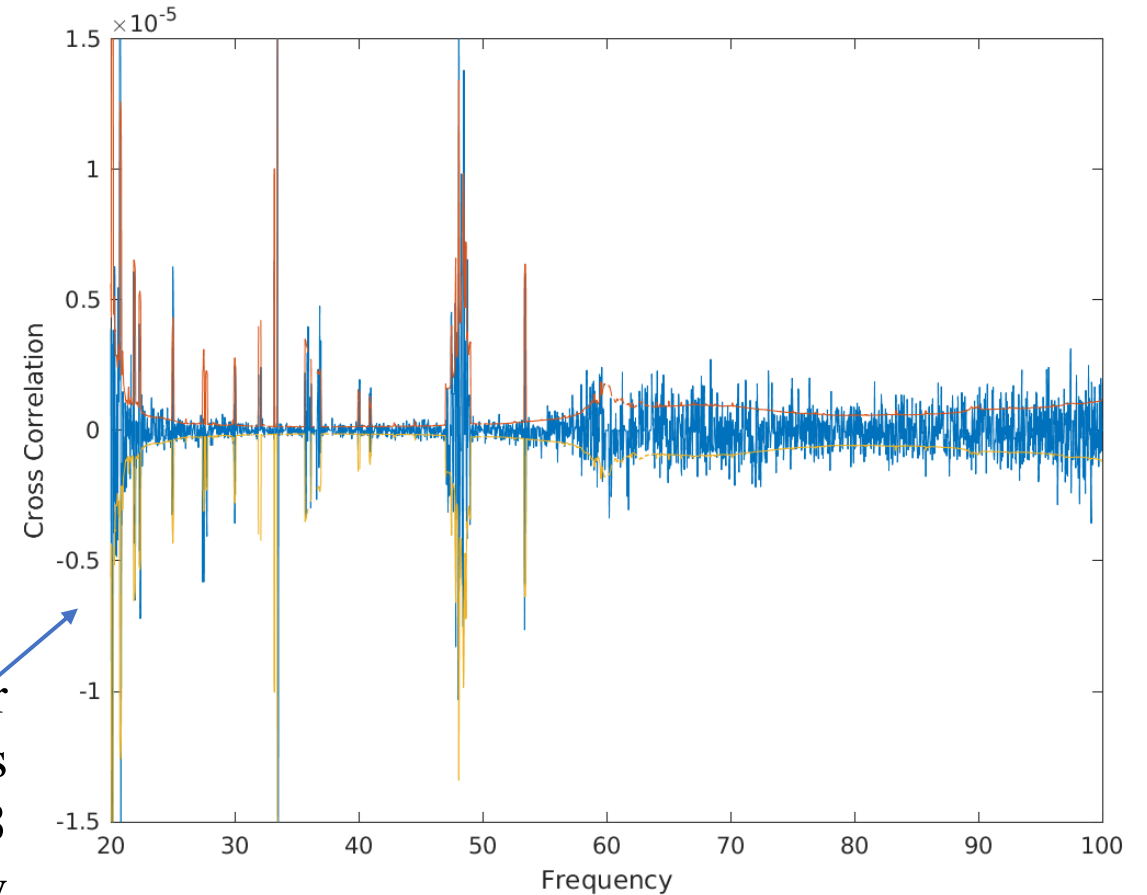


Plot showing the variation in the ratio of standard deviation in Ω with σ from the start of O3b analysis.

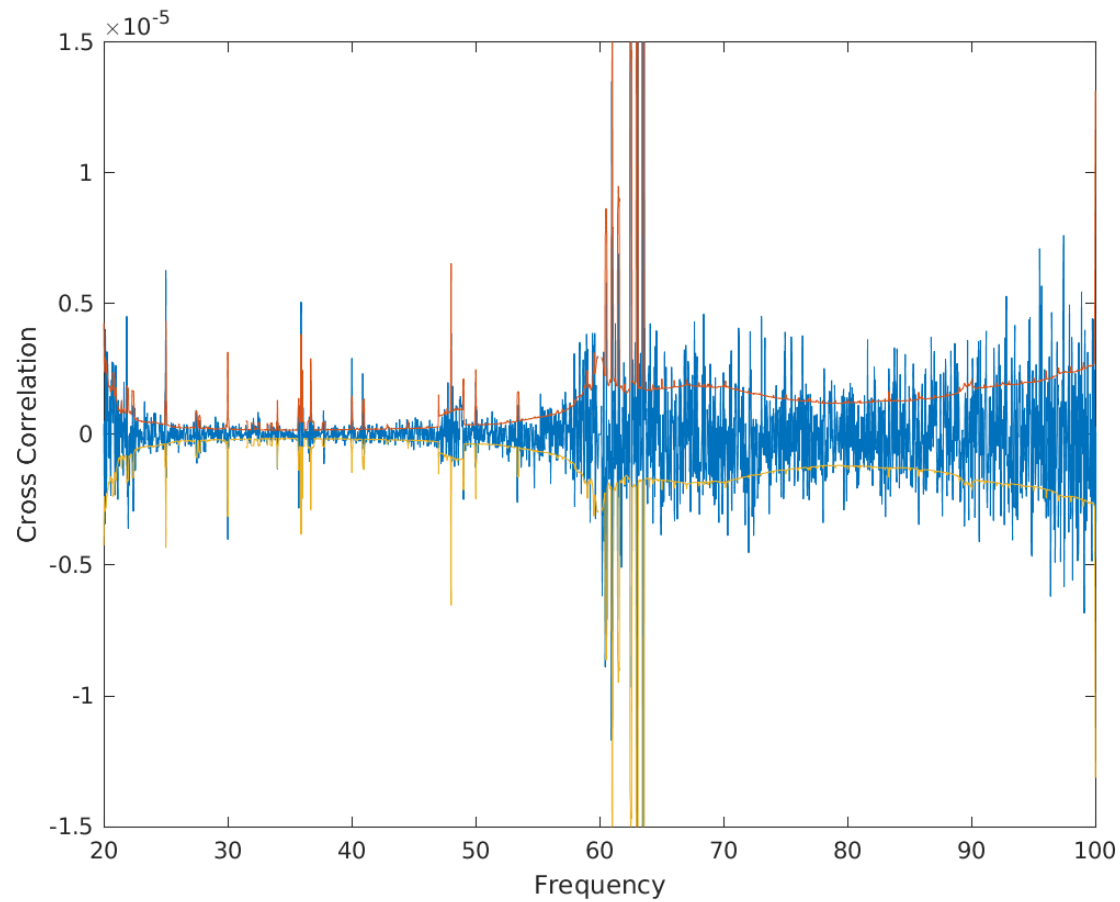
Plot showing the variation in σ from the start of O3b analysis. Red curve shows all dataset and orange is the data after $\delta\sigma$ cuts.



→ The cross-correlation spectrum obtained after combining the O3 run data from all detector pairs (HL, HV, LV), with a power-law index $\alpha = 0$ and $\pm 1 \sigma$ uncertainty level in the red and yellow line.

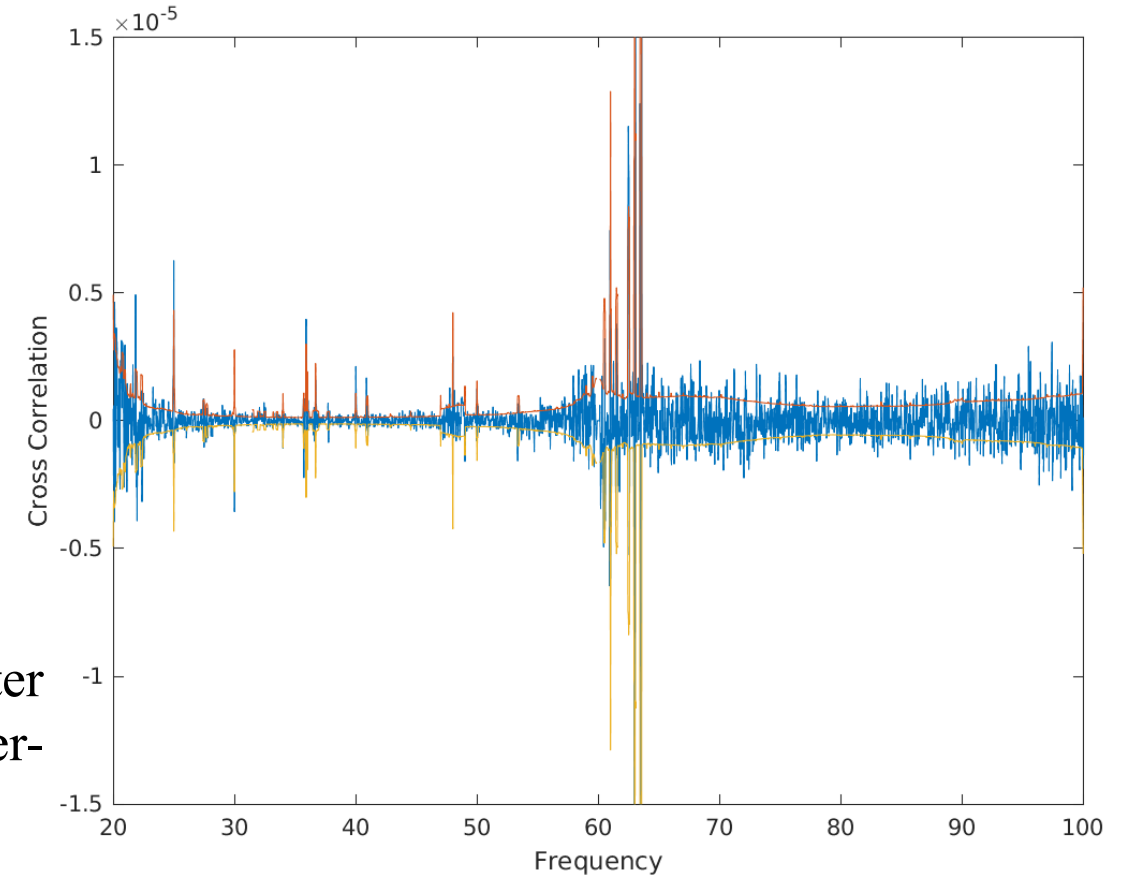


The cross-correlation spectrum obtained after combining the O3 run data from all detector pairs (HL, HV, LV), with a power-law index $\alpha = 2/3$ and $\pm 1 \sigma$ uncertainty level in the red and yellow line.



The cross-correlation spectrum obtained after combining the O1+O2+O3 run data with a power-law index $\alpha = 0$ and $\pm 1 \sigma$ uncertainty level.

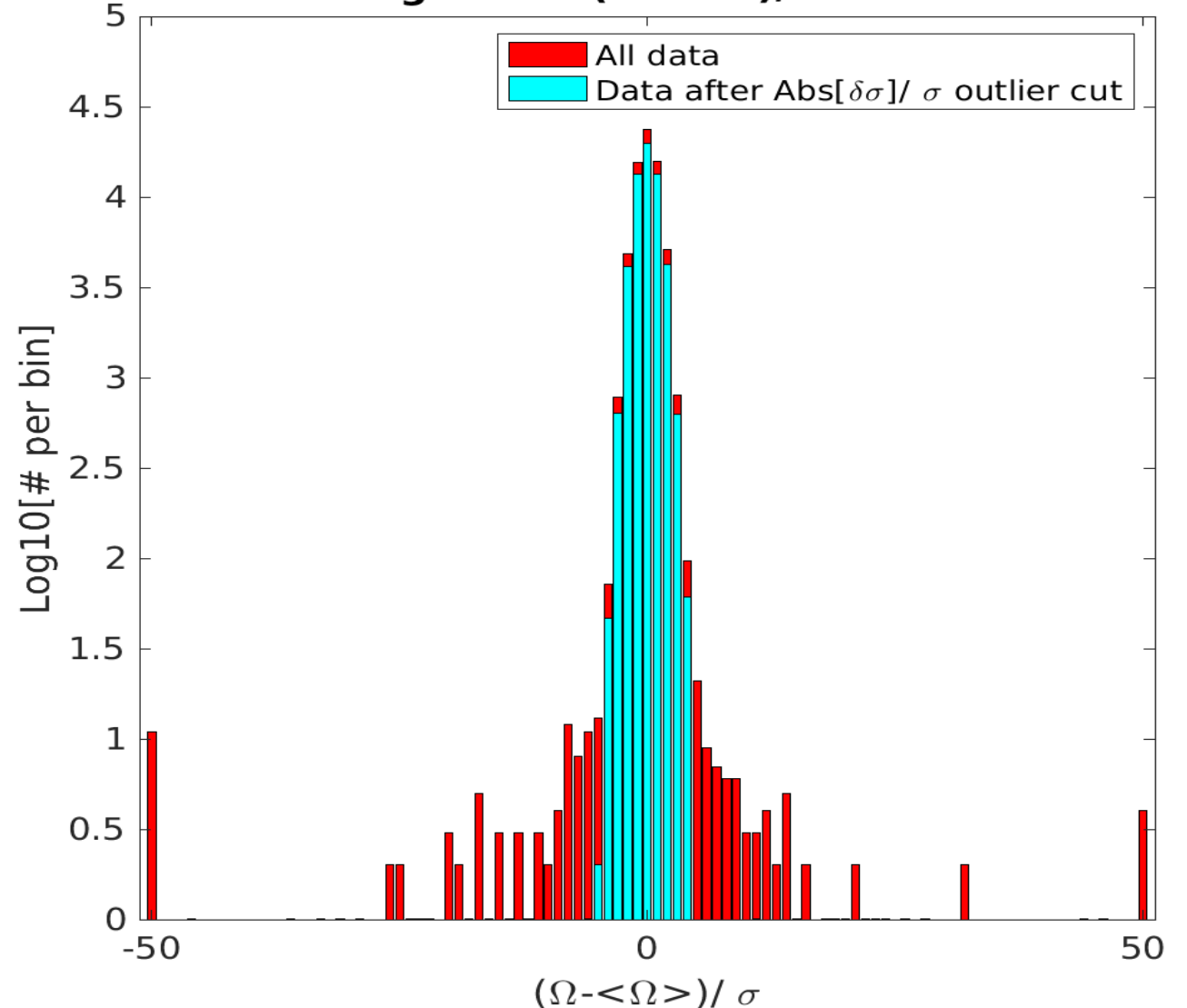
The cross-correlation spectrum obtained after combining the O1+O2+O3 run data with a power-law index $\alpha = 2/3$ and $\pm 1 \sigma$ uncertainty level.



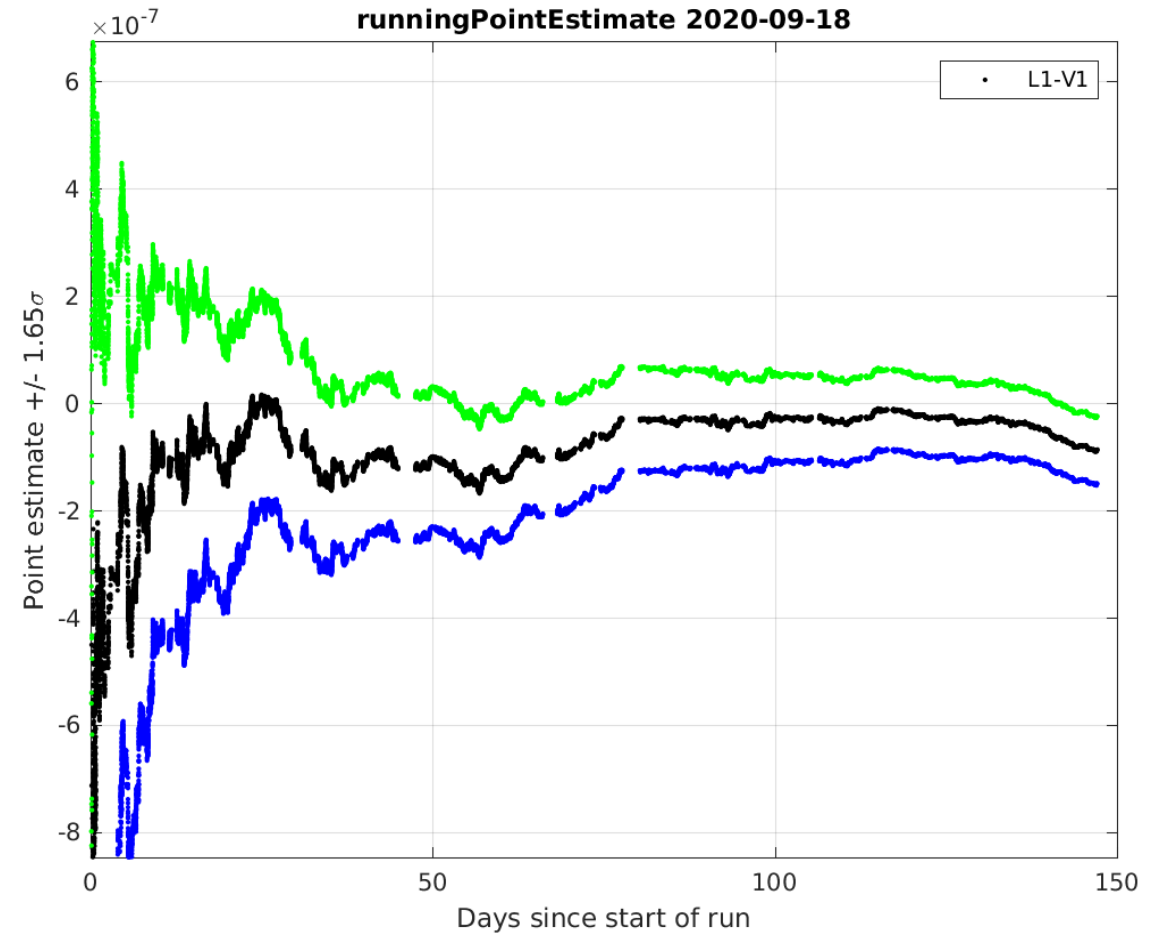
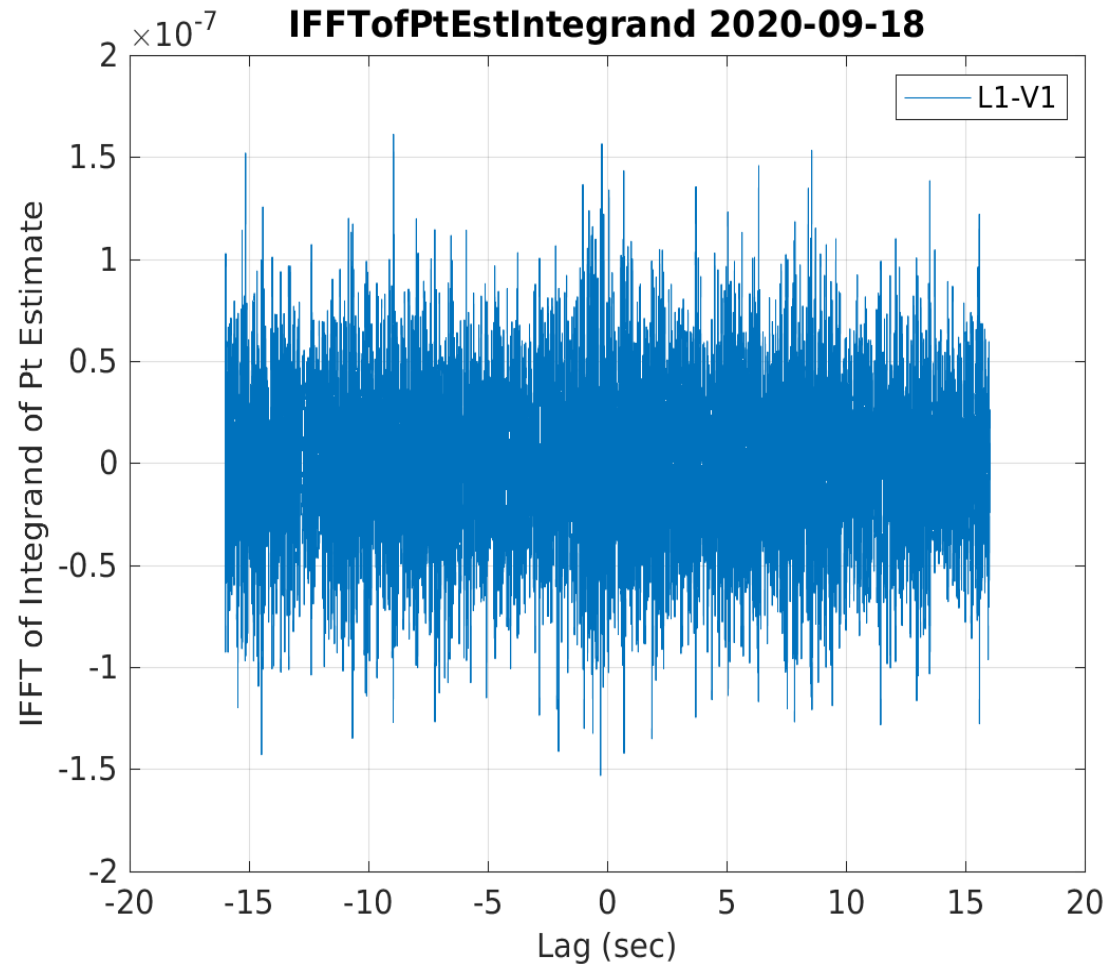
Point estimates and σ errors

- Histogram showing the distribution of excess residual noise (i.e. ratio between the standard deviation of Ω and the corresponding statistical errors σ_Ω) for LV detector pair data with 192 s segment duration for O3b dataset.

s from L1-V1: Histogram of $(\Omega - \langle \Omega \rangle) / \sigma$ with outlier cuts 20



- Point estimates and corresponding sigma errors for each detector pair used to set upper limits on Ω_{GW} .



Point estimates from O3 analysis

Power-law Index α	$f_{99\%}^{HL}$ (Hz)	$\hat{C}^{HL}/10^{-9}$	$f_{99\%}^{HV}$ (Hz)	$\hat{C}^{HV}/10^{-9}$	$f_{99\%}^{LV}$ (Hz)	$\hat{C}^{LV}/10^{-9}$
0	76.1	-2.1 ± 8.2	97.7	229 ± 98	88.0	-134 ± 63
2/3	90.2	-3.4 ± 6.1	117.8	145 ± 60	107.3	-82 ± 40
3	282.8	-1.3 ± 0.9	375.8	9.1 ± 4.1	388.0	-4.9 ± 3.1

Table:1 represents the isotropic SGWB searches with O3 data for power law index $\alpha = 0, \frac{2}{3}, 3$. Each detector pair contains 99% of the sensitivity in frequency band from 20 Hz to respective frequency level $f_{99\%}$.

LVC stochastic group, manuscript submitted to PRL
arXiv:2101.12130v1 [gr-qc]

Comparing O3 results with O1 and O2

Power-law Index α	O1 [1]	O2 [1]	O3	O1+O2+O3 [2]
0	$(4.4 \pm 6.0) \times 10^{-8}$	$(2.2 \pm 2.2) \times 10^{-8}$	$(-2.7 \pm 8.1) \times 10^{-9}$	$(1.1 \pm 7.5) \times 10^{-9}$
2/3	$(3.5 \pm 4.4) \times 10^{-8}$	$(2.0 \pm 1.6) \times 10^{-8}$	$(-3.7 \pm 6.0) \times 10^{-9}$	$(-0.2 \pm 5.6) \times 10^{-9}$
3	$(3.7 \pm 6.6) \times 10^{-9}$	$(3.5 \pm 2.8) \times 10^{-9}$	$(-1.1 \pm 0.9) \times 10^{-9}$	$(-0.6 \pm 0.8) \times 10^{-9}$

Table:2 shows the isotropic SGWB searches with O1, O2, O3 datasets and combined data with various power-law distribution choices $\alpha = 0, \frac{2}{3}, 3$. The values corresponding to α in O1, O2, O3 and O1+O2+O3 shows the point estimates and the corresponding $\pm 1 \sigma$ error values for the cross-correlation estimates \hat{C}_{IJ} .

[1] B.P. Abbott et al. PRD 100, 061101 (2019)

[2] LVC stochastic group, manuscript submitted to PRL
arXiv:2101.12130v1 [gr-qc]

Upper limits on Ω_{GW}

Power-Law Index α	Ω_{GW} from (O3 analysis) [2]	Ω_{GW} from (O2 analysis) [1]	Improvement factor
0	5.8×10^{-9}	3.5×10^{-8}	6.0
2/3	3.4×10^{-9}	3.0×10^{-8}	8.8
3	3.9×10^{-10}	5.1×10^{-9}	13.1

[1] B.P. Abbott et al. PRD 100, 061101 (2019)

[2] LVC stochastic group, manuscript submitted to PRL
arXiv:2101.12130v1 [gr-qc]

Conclusion

- I developed a method to take care of astrophysical background in 3G detectors.
- Subtraction-noise projection method is effective in reducing the residual noise data.
- Geometrical interpretation of matched filtering and parameter estimation is easy and realistic approach for such a method.
- Increasing the possibility of detecting a SGWB with 3G gravitational wave detectors ET and CE.
- The upper limits on SGWB from O3 stochastic analysis improved by a significant margin over the previous upper limits on SGWB.
- With future observations O4 (or O5?) these limits will improve further.

Subtraction cont...

- A foreground signal coming from N_s sources,

$$H(t) = \sum_{i=1}^{N_s} h_i(t)$$

- The norm squared of errors is (from Eq.(14))

$$\overline{\langle \delta H | \delta H \rangle} = N_p \times N_s$$

- Relative error in subtracting the whole foreground is

$$\frac{\delta H}{H} \approx \frac{\delta h}{h}$$

- Overlapping in binary signals can lead to degeneracy in parameter space, thus

$$\overline{\langle \delta H | \delta H \rangle} = N_p' \times N_s$$

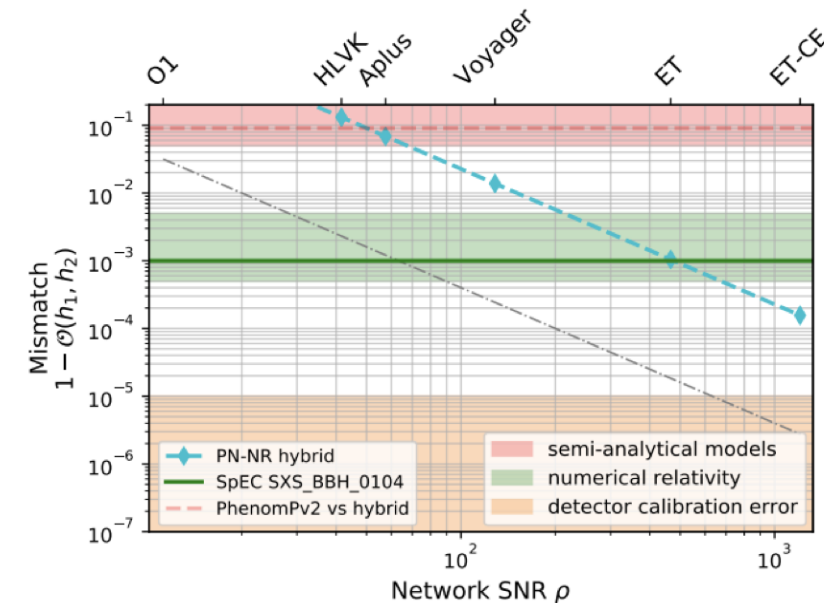
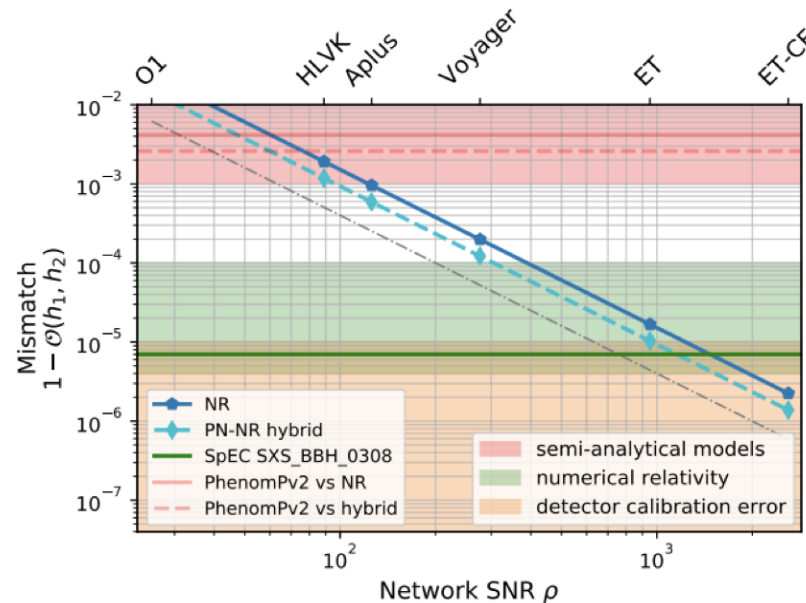
Waveform systematic errors

- Different waveforms can give rise to systematic uncertainties in the estimation of parameters.
- These systematic errors can be tested with
 - Repeated Bayesian analysis for different waveforms
 - Comparison of estimated parameters between waveform models.
 - Statistical errors in SNR
 - Response of detector network
- Mismatch between two waveforms is

$$1 - \mathcal{O}(h_1, h_2) < \frac{D}{2 \times \text{SNR}^2}$$

- SNR at which systematic and statistical errors are equal

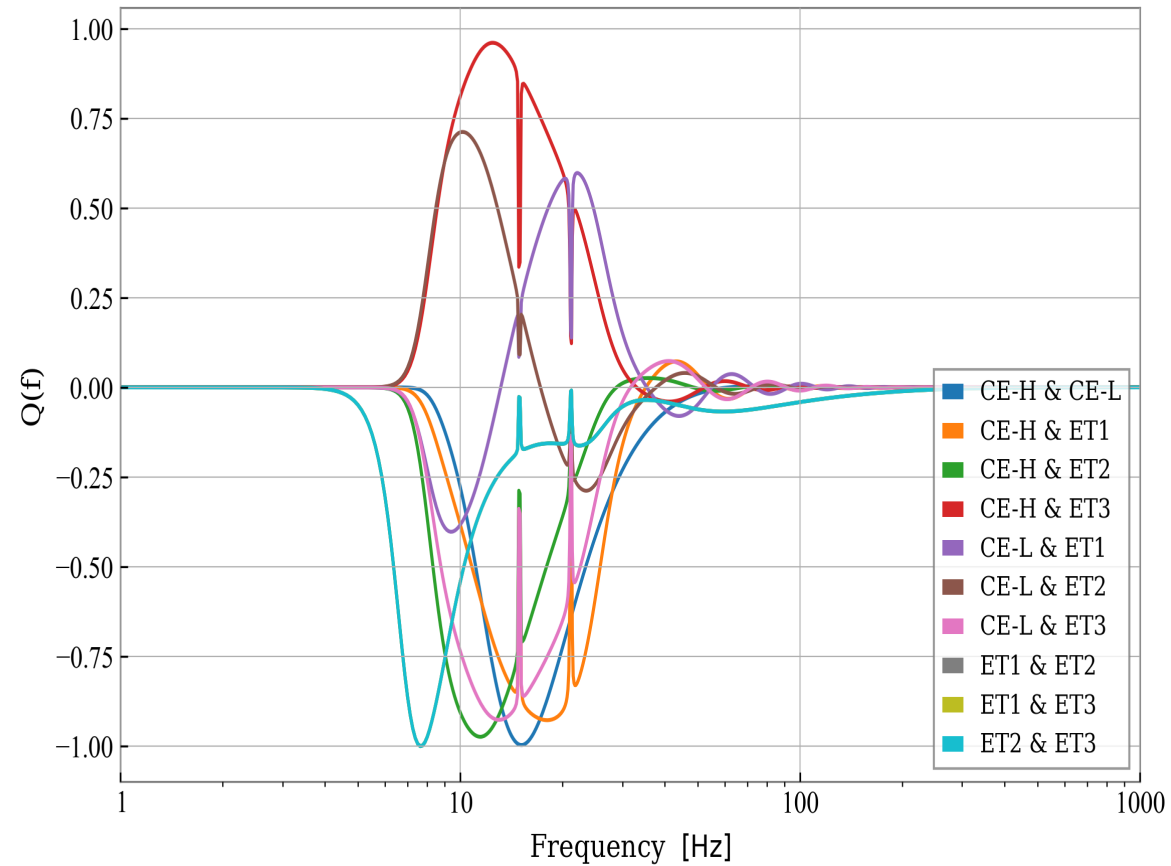
$$\rho_{eff} = \frac{1}{\sqrt{2}(1 - \mathcal{O}(h_{bf} - h_{true}))}$$



Predicted waveform accuracy for GW detectors

Optimal filter

$$Q_{IJ}(f) = \frac{\gamma_{IJ}(f)\Omega_{GW}(f)H_0^2}{f^3 P_I(f)P_J(f)}$$



- Different noise realization leads to different best-fit parameter estimation

$$\hat{\lambda} = \lambda^\alpha + \delta\lambda^\alpha$$

- Gaussian probability distribution

$$p(\delta\lambda^\alpha) \propto \mathcal{N} e^{-\frac{1}{2} \Gamma_{\alpha\beta} \delta\lambda^\alpha \delta\lambda^\beta}$$

- $\mathcal{N} = \sqrt{\det(\Gamma_{\alpha\beta}/2\pi)}$ is normalization constant.
- $\delta\lambda^\alpha \delta\lambda^\beta$ gives the variance and covariance matrix as

$$\overline{\delta\lambda^\alpha \delta\lambda^\beta} = \Gamma^{\alpha\beta} + \mathcal{O}(SNR)^{-1}$$

- $\Gamma^{\alpha\beta}$ gives the variance of α and β with respect to each other.

- To optimally filter data, unbiased estimator of true signal is

$$h' = \sum_i \zeta_i s_i$$

Which follows $\langle h' \rangle = h$, implies that $\sum_i \zeta_i = 1$ must hold for minimum variance (i.e. minimum unbiased estimator is unique).

- Thus the minimum variance in h is

$$\sigma_h^2 = \sum_i \zeta_i^2 \sigma_i^2 = \text{minimum}$$

where

$$\zeta_i = \left(\sum_j \frac{1}{\sigma_j^2} \right)^{-1} \frac{1}{\sigma_i^2}$$

represents the linear combination of weighted average, giving less weight to noisy measurements which have large variance. i & j runs over the different measurements of the detector.

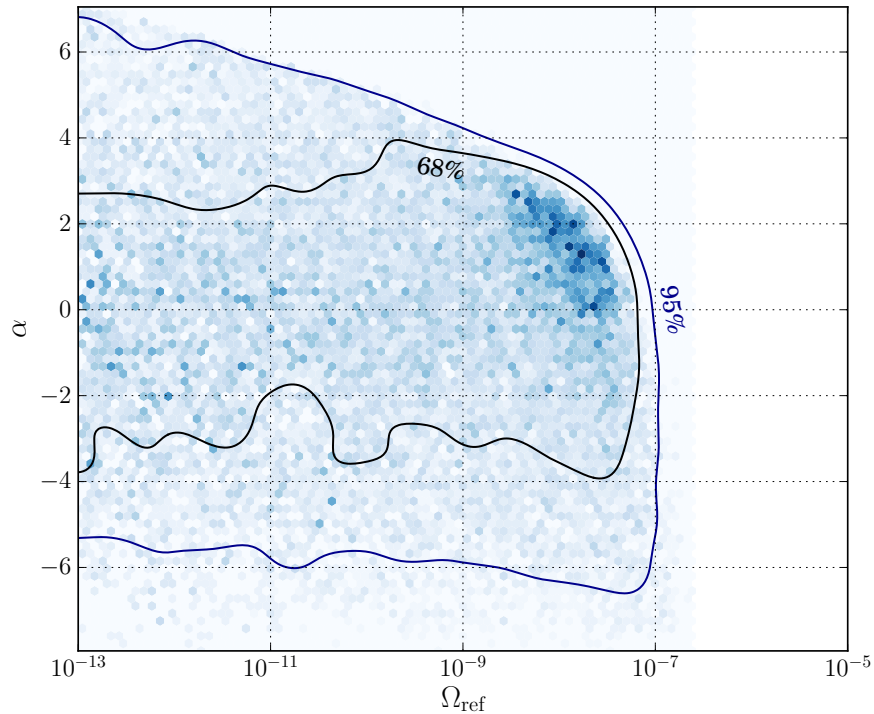
- Therefore, the linear combination is

$$h = \left(\sum_j \frac{1}{\sigma_j^2} \right)^{-1} \left(\sum_i \frac{s_i}{\sigma_i^2} \right)$$

Limits from O2 run

- **Astrophysical backg. limits** 4.8×10^{-8} (f = 20-92 Hz)
- **Cosmological backg. limits** 6.0×10^{-8} (f = 20-82 Hz)

For $\alpha = 0$



For $\alpha = 2/3$

